

The Hall effect in star formation

C. R. Braiding^{*} and M. Wardle

Research Centre in Astronomy, Astrophysics and Astrophotonics

Department of Physics and Astronomy, Macquarie University, Sydney, NSW 2109, Australia

Modified: 2012 January 18

ABSTRACT

Magnetic fields play an important role in star formation by regulating the removal of angular momentum from collapsing molecular cloud cores. Hall diffusion is known to be important to the magnetic field behaviour at many of the intermediate densities and field strengths encountered during the gravitational collapse of molecular cloud cores into protostars, and yet its role in the star formation process is not well-studied. We present a semianalytic self-similar model of the collapse of rotating isothermal molecular cloud cores with both Hall and ambipolar diffusion, and similarity solutions that demonstrate the profound influence of the Hall effect on the dynamics of collapse.

The solutions show that the size and sign of the Hall parameter can change the size of the protostellar disc by up to an order of magnitude and the protostellar accretion rate by fifty per cent when the ratio of the Hall to ambipolar diffusivities is varied between $-0.5 \leq \eta_H/\eta_A \leq 0.2$. These changes depend upon the orientation of the magnetic field with respect to the axis of rotation and create a preferred handedness to the solutions that could be observed in protostellar cores using next-generation instruments such as ALMA.

Hall diffusion also determines the strength and position of the shocks that bound the pseudo and rotationally-supported discs, and can introduce subshocks that further slow accretion onto the protostar. In cores that are not initially rotating (not examined here), Hall diffusion can even induce rotation, which could give rise to disc formation and resolve the magnetic braking catastrophe. The Hall effect clearly influences the dynamics of gravitational collapse and its role in controlling the magnetic braking and radial diffusion of the field merits further exploration in numerical simulations of star formation.

Key words: accretion discs – MHD – stars: formation.

1 INTRODUCTION

Low-mass stars form by the gravitational collapse of molecular cloud cores over many orders of magnitude in size and density. Cores form within molecular clouds as a result of turbulent fluctuations, and they gradually contract as ambipolar diffusion erodes the magnetic support (e.g. Tasker & Tan 2009; Federrath et al. 2010). Turbulence may also support the core against collapse and its decay can aid in triggering star formation (e.g. Mac Low & Klessen 2004; Ballesteros-Paredes et al. 2007). The core becomes unstable when the mass-to-flux ratio exceeds the critical value

$$\left(\frac{M}{\Phi}\right)_{crit} = \frac{C_\Phi}{G^{1/2}} \quad (1)$$

where C_Φ is a dimensionless (in cgs units) numerical coefficient that depends upon the magnetic field and density dis-

tributions (Mestel & Spitzer 1956; Mouschovias & Spitzer 1976; McKee et al. 1993).

The core collapses dynamically into what is termed a “pseudodisc” (Galli & Shu 1993a,b), which has a flattened shape due to the material falling in preferentially along the magnetic field lines. The field is effectively frozen into the cloud, and the infalling material is deflected by the field lines towards the equatorial plane. The pseudodisc contracts dynamically in the radial direction, dragging the field lines into a split monopole (hourglass) configuration (Galli & Shu 1993a,b) that is consistent with observations of the polarisation of dust continuum emission in cores (Cortes & Crutcher 2006; Girart et al. 2006; Gonçalves et al. 2008; Attard et al. 2009). The build up in magnetic pressure acts as an impediment to further collapse, however, the magnetic tension in the envelope never suffices to suspend the envelope against the gravity of the growing protostar (Allen et al. 2003a,b).

Within the pseudodisc ambipolar diffusion becomes important (Desch & Mouschovias 2001), leading to a decou-

^{*} E-mail: catherine.braiding@gmail.com

pling of the magnetic field from the neutral gas, which takes place within an outwardly-propagating MHD shock (Li & McKee 1996). This shock (referred to as the “magnetic diffusion shock” in this work) is a continuous transition in the magnetic field and density (Krasnopolsky & Königl 2002, hereafter KK02), inwards of which the neutral material falls in at a near-free fall speed due to the reduced magnetic support. The centrifugal force becomes important and triggers the formation of a hydrodynamic shock that strongly decelerates the infalling matter and allows a Keplerian disc to form (Shu et al. 1987). A disc wind or jet may form, launched from the inner regions of the collapse (Königl 1989; Tomisaka 2002; Allen et al. 2003b).

Angular momentum is removed from the pseudodisc by the twisting of magnetic field lines, which transport angular momentum from the inner parts of the core towards its outer regions (Basu & Mouschovias 1994). The amount of magnetic braking affecting the collapse, and hence the existence and sign of the Keplerian protostellar disc, is determined by the coupling of the field to the charged particles and the drift of these against the neutral component in response to the electric field in the neutral rest frame. The Lorentz force is transmitted to the neutral gas through the drag forces caused by collisions between the neutral and charged particles (e.g. Königl & Salmeron 2011).

Simulations of star formation typically approximate the magnetic field behaviour by ideal magnetohydrodynamics (IMHD), where the mass-to-flux ratio is held constant and the magnetic field is regarded as being frozen into the neutral medium (e.g. Galli et al. 2006; Mellon & Li 2008; Machida et al. 2008a). In this situation the magnetic field and the particles move together in the collapsing flow, however this simplification only truly applies in the outermost regions of gravitational collapse where the density is low. If IMHD were to hold true throughout the collapse the magnetic flux in the star would be 10^3 – 10^5 times larger than that observed in young stars (this is the “magnetic flux problem”, described in Chandrasekhar & Fermi 1953).

As the density in the core increases flux freezing breaks down, and the relative drifts of different charged species with respect to the neutral particles delineate three magnetic diffusivity regimes:

- the *Ohmic (resistive) diffusion* limit, which dominates in high density regions where the ionisation fraction is low. The ions and the electrons frequently collide with the neutrals over the electron gyration period, and the magnetic field is decoupled from all charged particles. Ohmic diffusion is important in the innermost regions of the protostellar disc where the density and collisional rates are high (e.g. Shu et al. 2006; Machida et al. 2008b).
- the *ambipolar diffusion* limit, which dominates in regions of relatively low density where the fractional ionisation is high, causing the ionised component to drift with the field through the neutrals. Ambipolar diffusion is dominant in molecular clouds (Wardle 2007), in protostellar discs at radial distances beyond ~ 10 au and close to the surface of these discs nearer to the protostar (Salmeron 2009).
- the *Hall diffusion* limit, which dominates in the intermediate regimes between ambipolar and Ohmic diffusion. The more massive particles such as ions and charged dust grains are decoupled from the magnetic field and are instead

collisionally-coupled to the neutral gas. Hall diffusion is expected to dominate in many regions of molecular clouds as they undergo gravitational collapse (Wardle 2004a), and in protostellar discs (Sano & Stone 2002a,b).

In the Hall limit the magnetic response of the disc is not invariant under a global reversal of the magnetic field (Wardle & Ng 1999) as Hall diffusion twists the field and changes the angular momentum of the neutral fluid; in a rotationally-supported disc this causes the gas to fall inwards if it loses angular momentum, or outwards if it gains it. Ambipolar and Ohmic diffusion, however, always cause the field to move in the radial direction against the flow of the neutrals – reversing the direction of the field does not affect the direction of the field diffusion.

The actual magnitude and type of coupling that occurs between the fluid and magnetic field in molecular clouds and protostellar discs is uncertain due to the difficulty in obtaining detailed observations in these regions, particularly of the magnetic field. Calculations of the ionisation equilibrium and resistivity by Wardle (2004a) suggested that Hall diffusion is important and may dominate the magnetic field behaviour at many of the densities and field strengths encountered in molecular clouds and protostellar discs. In particular, the Hall term is significant for molecular gas densities in the range $\sim 10^8$ – 10^{11} cm $^{-3}$ (when B scales as $B \propto n_{\text{H}}^{1/4}$), although the presence and distribution of grains complicates the calculation of the diffusivities (Wardle & Ng 1999).

In simulations of star formation where the magnetic field behaviour is not governed by IMHD it is usually ambipolar diffusion that is included (e.g. Ciolek & Königl 1998; Adams & Shu 2007; Mellon & Li 2009). Ohmic diffusion is important in the innermost regions of the collapse as the density builds up, particularly when $\rho > 10^{11}$ cm $^{-3}$ (Shu et al. 2006). It seems likely that star formation requires all of these processes to some degree, however it is only recently that simulations have been performed with more than one of these processes included (Li et al. 2011), and Hall diffusion is almost always overlooked. The nature of the coupling determines the magnetic field direction as the field lines emerge from the surface of the protostellar disc, which in turn controls the amount of material that is able to slide along the field lines and be flung outwards from the surface in disc-driven wind models (Wardle & Königl 1993; Wardle 2004b).

In this paper we construct a semianalytic model of gravitational collapse in order to demonstrate the importance of Hall diffusion and its influence on the magnetic braking catastrophe, in which the magnetic braking affecting a collapsing flow is such that all angular momentum is removed from the flow and no Keplerian disc may form. The paper is organised as follows: in §2 we describe the formulation of the self-similar collapse equations, the assumptions governing this approximation and the boundary conditions of the core; the numerical procedures are outlined in §3; in §4 we present the similarity solutions; the effect of the Hall term on the solutions and the magnetic braking catastrophe is discussed in §5 and our conclusions are stated in §6.

2 FORMULATION

The goal of this work is to construct a semianalytic model of gravitational collapse similar to that of KK02, including terms for Hall diffusion in the equations for the magnetic field diffusion and braking. This allows the calculation of similarity solutions that show the importance of Hall diffusion in molecular cloud cores and collapsing flows, as well as comparisons between the influence of the Hall and ambipolar diffusion terms. Following KK02, the magnetohydrodynamic equations for the isothermal system are given by

$$\frac{\partial \rho}{\partial t} + \nabla \cdot (\rho \mathbf{V}) = 0, \quad (2)$$

$$\rho \frac{\partial \mathbf{V}}{\partial t} + \rho (\mathbf{V} \cdot \nabla) \mathbf{V} = -\nabla P + \rho \mathbf{g} + \mathbf{J} \times \mathbf{B}, \quad (3)$$

$$\nabla^2 \Phi = 4\pi G \rho, \quad (4)$$

$$\nabla \cdot \mathbf{B} = 0, \quad (5)$$

and

$$\frac{\partial \mathbf{B}}{\partial t} = \nabla \times (\mathbf{V} \times \mathbf{B}) - \nabla \times \left[\eta (\nabla \times \mathbf{B}) + \eta_H (\nabla \times \mathbf{B}) \times \hat{\mathbf{B}} + \eta_A (\nabla \times \mathbf{B})_{\perp} \right], \quad (6)$$

where ρ is the gas density, \mathbf{V} the velocity field, P the pressure, \mathbf{g} the gravitational field, Φ the gravitational potential, c the speed of light, \mathbf{J} the current density, \mathbf{B} the magnetic field, and η and $\eta_{H,A}$ are the diffusion coefficients for the Ohmic, Hall and ambipolar terms in the induction equation.

We assume that the collapse is axisymmetric to simplify the calculations, and the magnetic field is taken to be aligned with the axis of rotation. This is in contrast with some observations of protostellar systems such as the binary NGC 1333 IRAS 4A where the axis normal to the binary envelope lies between the outflow and magnetic field axes (Girart et al. 2006; Attard et al. 2009), however most observations seem to show that the magnetic field takes on an hourglass shape that is aligned with the axis of rotation (e.g. Vink et al. 2005; Cortes & Crutcher 2006). Alignment is required by the assumption of axisymmetry, as misalignment introduces three-dimensional effects that cannot be modelled here.

Using cylindrical coordinates, the mass, radial momentum and angular momentum conservation equations, as well as the hydrostatic equilibrium equation, the solenoidal condition and the vertical component of the induction equation are, under the assumptions of isothermality (that $P = \rho c_s^2$) and axisymmetry:

$$\frac{\partial \rho}{\partial t} + \frac{1}{r} \frac{\partial}{\partial r} (r \rho V_r) = -\frac{\partial}{\partial z} (\rho V_z), \quad (7)$$

$$\rho \frac{\partial V_r}{\partial t} + \rho V_r \frac{\partial V_r}{\partial r} = \rho g_r - c_s^2 \frac{\partial \rho}{\partial r} + \rho \frac{V_\phi^2}{r} + \frac{B_z}{4\pi} \frac{\partial B_r}{\partial z} - \frac{\partial}{\partial r} \left(\frac{B_z^2}{8\pi} \right) - \frac{1}{8\pi r^2} \frac{\partial}{\partial r} (r B_\phi)^2 - \rho V_z \frac{\partial V_r}{\partial z}, \quad (8)$$

$$\begin{aligned} \rho \frac{\partial}{\partial t} (r V_\phi) + \frac{\rho V_r}{r} \frac{\partial}{\partial r} (r V_\phi) \\ = \frac{B_z}{4\pi} \frac{\partial B_\phi}{\partial z} + \frac{B_r}{4\pi r} \frac{\partial}{\partial r} (r B_\phi) - \rho V_z \frac{\partial}{\partial z} (r V_\phi), \end{aligned} \quad (9)$$

$$\begin{aligned} \rho \frac{\partial V_z}{\partial t} + \rho V_r \frac{\partial V_z}{\partial r} + \rho V_z \frac{\partial V_z}{\partial z} + c_s^2 \frac{\partial \rho}{\partial z} \\ = \rho g_z - \frac{\partial}{\partial z} \left(\frac{B_\phi^2}{8\pi} + \frac{B_r^2}{8\pi} \right) + \frac{B_r}{4\pi} \frac{\partial B_z}{\partial r}, \end{aligned} \quad (10)$$

$$\frac{\partial B_z}{\partial z} = -\frac{1}{r} \frac{\partial}{\partial r} (r B_r) \quad (11)$$

and

$$\begin{aligned} \frac{\partial B_z}{\partial t} = -\frac{1}{r} \frac{\partial}{\partial r} \left[r \left(V_r B_z + \left[\eta (\nabla \times \mathbf{B}) + \frac{\eta_H}{B} (\nabla \times \mathbf{B}) \times \mathbf{B} \right. \right. \right. \\ \left. \left. \left. - \frac{\eta_A}{B^2} ((\nabla \times \mathbf{B}) \times \mathbf{B}) \times \mathbf{B} \right) \right] \right]_\phi \end{aligned} \quad (12)$$

where g_r and g_z are the radial and vertical components of the gravitational field, and c_s is the isothermal sound speed given by $c_s = (k_B T / m_n)^{1/2} \approx 0.19 \text{ km s}^{-1}$ (with k_B the Boltzmann constant, T the gas temperature, typically taken to be 10 K, and m_n the mean mass of a gas particle). The assumption of isothermality breaks down due to radiative trapping when the central density reaches $\sim 10^{10} \text{ cm}^{-3}$ (Gaustad 1963), which occurs on scales $r \lesssim 5 \text{ au}$ for a typical simulation. It is expected that isothermality shall break down in the innermost regions of our solutions, however, as thermal stresses do not play a significant role in the larger-scale dynamics isothermality is not expected to introduce large errors into the calculations.

The disc is assumed to be thin based upon the results of Mouschovias and collaborators (e.g. Fiedler & Mouschovias 1992, 1993), which have shown that an initially-uniform, self-gravitating, magnetised molecular cloud core rapidly collapses along the magnetic field lines. This assumption allows us to further reduce the dimensionality of the problem by vertically-averaging the variables over the scale height of the disc, although it implies that processes that depend on variations in the density or the magnetic field with height within the disc cannot be included in the collapse calculations. Effects such as turbulence or the interaction between active and dead zones in the disc are not expected to have a large effect on the overall dynamics of early collapse (although they are known to become important in some regions of protostellar discs once the adiabatic core and protostar have formed) and their exclusion is necessary to the self-similarity of the solutions.

The vertical averaging is performed as in KK02. As only the vertical component of the induction equation and our equation for the magnetic braking differ from theirs, we perform the integration of these in Appendix A and refer the reader to their appendix A for the others. The quantities η , η_H/B and η_A/B^2 are approximated as being constant with height, as are the radial velocity, the azimuthal velocity and the radial component of gravity.

The disc is threaded by an open magnetic field possessing an even symmetry, so that $B_r = B_\phi = 0$ at the disc midplane. The radial and toroidal field components are taken to scale with height as

$$B_r(r, z) = B_{r,s}(r) \frac{z}{H(r)} \quad (13)$$

$$B_\phi(r, z) = B_{\phi,s}(r) \frac{z}{H(r)} \quad (14)$$

where $H(r)$ is the scale height of the disc and $B_{r,s}$ and $B_{\phi,s}$

are the magnetic field components at the surface of the disc; these scalings are motivated by the field configuration of a rotationally-supported thin disc in which the field is well-coupled to the gas (Wardle & Königl 1993). As ambipolar diffusion and Hall diffusion become more important in the inner regions of the disc where the field is less well-coupled to the gas, this approximation is no longer adequate, however none of the dominant terms in the equation set depend upon the particulars of the vertical variation of the field within the disc (KK02), so it remains reasonable to adopt these scalings across the domain of self-similar collapse.

The surface density of the pseudodisc is defined by the expression

$$\Sigma = \int_{-\infty}^{\infty} \rho dz = 2H\rho, \quad (15)$$

assuming that the density is constant with height within the disc, and the specific angular momentum is defined by $J = rV_\phi$. We neglect any mass loss due to a disc wind. The radial components of gravity and the magnetic field are calculated using the monopole expressions

$$g_r = -\frac{GM(r)}{r^2} \quad (16)$$

and

$$B_{r,s} = \frac{\Psi(r,t)}{2\pi r^2}, \quad (17)$$

where the enclosed mass $M(r) \approx M_c$ when the central mass dominates and Ψ is the magnetic flux enclosed within the radius r . These simplifications were also used by KK02, as Contopoulos et al. (1998) found that these expressions give values of the gravitational force and magnetic field that are near enough to those found using an iterative method that they do not introduce significant errors into the calculation.

The vertical angular momentum transport above and within the disc is achieved by magnetic braking, especially during the dynamic collapse phase inwards of the magnetic diffusion shock and in the rotationally-supported inner disc. The approach to modelling the magnetic braking used in this work, which is described in more detail in Appendix A, is adapted from that of Basu & Mouschovias (1994) for the pre-point mass formation collapse phase. This formulation is not well-defined in the innermost rotationally-supported regions of the pseudodisc, where the calculated magnetic braking becomes stronger than is expected and the angular momentum transport is expected to be dominated by a disc wind (which is not included but discussed further in §5).

A cap is then placed upon the azimuthal magnetic field component in order to ensure that it does not greatly exceed the vertical component; balancing the torques on the disc then allows us to define

$$B_{\phi,s} = -\min \left[\frac{\Psi}{\pi r^2} \left(\frac{r\Omega - r\Omega_b}{V_{A,\text{ext}}} \right); \delta B_z \right]; \quad (18)$$

where δ is a constant parameter ($= 1$ in our solutions) that limits the magnetic braking, Ω is the local angular velocity, and Ω_b is the background angular velocity of the cloud, which is small compared to that of the core. $V_{A,\text{ext}}$ is the Alfvén wave speed in the external medium, which is parameterised with respect to the sound speed using

$$\alpha = c_s/V_{A,\text{ext}}, \quad (19)$$

where again α is a constant parameter of the model. We take $\alpha = 0.08$ in the solutions presented here, which is a reasonable approximation as the observations of Crutcher (1999) indicated that $V_{A,\text{ext}} \approx 1 \text{ km s}^{-1}$ over many orders of magnitude in several molecular clouds. The negative sign of $B_{\phi,s}$ and positive sign of δ are based on the assumption that there is no counter-rotation of material in the collapse; were the fluid counter-rotating then the signs of δ and $B_{\phi,s}$ would both change. The azimuthal drift velocity of the magnetic field is averaged over the disc scale height in Appendix A to give the final form of Equation A37 shown below.

The disc equations are further simplified by recognising that the thin disc approximation implies that terms of order $\mathcal{O}(H/r)$ are small in comparison to the other terms and can then be dropped from the equations. As in KK02, the only term of order $\mathcal{O}(H/r)$ that is kept is the combination $[B_{r,s} - H(\partial B_z/\partial z)]$, which occurs in the radial momentum equation and is important in refining the structure of the magnetic diffusion shock. This term is then retained in all of the equations in which it appears.

Taking all of these into account then gives the simplified set of equations:

$$\frac{\partial \Sigma}{\partial t} + \frac{1}{r} \frac{\partial}{\partial r} (r \Sigma V_r) = 0, \quad (20)$$

$$\frac{\partial V_r}{\partial t} + V_r \frac{\partial V_r}{\partial r} = g_r - \frac{c_s^2}{\Sigma} \frac{\partial \Sigma}{\partial r} + \frac{B_z B_{r,s}}{2\pi \Sigma} + \frac{J^2}{r^3}, \quad (21)$$

$$\frac{\partial J}{\partial t} + V_r \frac{\partial J}{\partial r} = \frac{r B_z B_{\phi,s}}{2\pi \Sigma}, \quad (22)$$

$$\frac{\Sigma c_s^2}{2H} = \frac{\pi}{2} G \Sigma^2 + \frac{GM_c \Sigma H}{4r^3} + \frac{1}{8\pi} (B_{r,s}^2 + B_{\phi,s}^2), \quad (23)$$

$$\frac{H}{2\pi} \frac{\partial \Psi}{\partial t} = -r H V_r B_z - \eta B_{r,s} - \frac{r \eta H}{B} B_z B_{\phi,s} - \frac{r \eta A}{B^2} B_{r,s} B_z^2 \quad (24)$$

and

$$B_{\phi,s} = -\min \left[\frac{\Psi \alpha}{\pi r^2 c_s} \left[\frac{J}{r} - \frac{\eta H}{B} \left(B_{r,s} - H \frac{\partial B_z}{\partial r} \right) \right] \right. \\ \left. \left[1 + \frac{\Psi \alpha}{\pi r^2 c_s} \frac{\eta_F B_z}{B^2 H} \right]^{-1}; \delta B_z \right], \quad (25)$$

along with Equations 16 and 17.

2.1 Self-Similarity

At any instant in time the collapse solutions look like stretched versions of themselves at previous times; this fractal-like behaviour is referred to as self-similarity. The pseudodisc forms as a collapse wave (referred to as the magnetic diffusion shock) propagates outwards at the speed of sound. The self-similarity of the waves of infall occurs because of the lack of characteristic time and length scales in the flow.

Gravitational collapse occurs over many orders of magnitude in radius and density, so that the point mass has negligible dimensions in comparison with the accretion flow.

The only dimensional quantities that effect the flow are the magnetic field \mathbf{B} , the diffusion coefficients η and $\eta_{H,A}$, the gravitational constant G , the isothermal sound speed c_s , the local radius r and the instantaneous time t ; this means that, except for scaling factors, all of the flow variables may be written as functions of a similarity variable defined by

$$x = \frac{r}{c_s t}. \quad (26)$$

KK02 noted that for a typical value of the sound speed ($c_s = 0.19 \text{ km s}^{-1}$ at $T = 10 \text{ K}$), $x = 1$ corresponds to a distance of $r \approx 6 \times 10^{15} \text{ cm}$ (400 au) when $t = 10^4 \text{ yr}$ (which is the characteristic age of a Class 0 YSO) and to a distance of $r \approx 6 \times 10^{16} \text{ cm}$ (4,000 au) when $t = 10^5 \text{ yr}$ (the age of a Class 1 YSO). The Class 0 YSO IRAM 04191 has a dense inner disc-like structure that resembles a tilted ring with an average radius of $r_0 \sim 1400 \text{ au}$ (Lee et al. 2005) — this is of the same order of magnitude as the centrifugal shock radius in the disc-forming solutions at the same age.

The physical quantities are expressed as the product of a nondimensional flow variable that depends only upon x and a dimensional part constructed from c_s , G and t :

$$\Sigma(r, t) = \left(\frac{c_s}{2\pi G t} \right) \sigma(x), \quad (27)$$

$$g_r(r, t) = \left(\frac{c_s}{t} \right) g(x), \quad (28)$$

$$V_r(r, t) = c_s u(x), \quad (29)$$

$$H(r, t) = c_s t h(x), \quad (30)$$

$$V_\phi(r, t) = c_s v(x), \quad (31)$$

$$J(r, t) = c_s^2 t j(x), \quad (32)$$

$$M(r, t) = \left(\frac{c_s^3 t}{G} \right) m(x), \quad (33)$$

$$\dot{M}(r, t) = \left(\frac{c_s^3}{G} \right) \dot{m}(x), \quad (34)$$

$$\mathbf{B}(r, t) = \left(\frac{c_s}{G^{1/2} t} \right) \mathbf{b}(x), \quad (35)$$

$$\Psi(r, t) = \left(\frac{2\pi c_s^3 t}{G^{1/2}} \right) \psi(x), \quad (36)$$

$$\text{and } \eta_{H,A} = c_s^2 t \eta'_{H,A}. \quad (37)$$

These equations have the same form and use the same notation as those in KK02, with the addition of extra diffusion coefficients to model the magnetic field more completely.

The Ohmic and ambipolar diffusion terms scale together, to a zeroth-order approximation, as they possess a similar dependence upon B and appear in the induction equation and the equation for the azimuthal field component multiplied by the same magnetic field terms. Because the field within the thin disc is effectively vertical, both ambipolar and Ohmic diffusion influence the field drift in the same manner. While one type of diffusion may dominate over the other at any individual point in the disc (in general, ambipolar diffusion in the outer regions where the density is low and Ohmic diffusion in the inner regions where the density is high; Wardle 2007), only one term is needed in order to study the change in the disc behaviour introduced by the Hall diffusion term that is of most interest in this work. The Ohmic and ambipolar diffusion terms are combined into a single term parameterised by the dimensionless constant $\tilde{\eta}_A$, referred to as the ambipolar diffusion parameter.

The ambipolar diffusion coefficient in a molecular cloud core without grains is given by the equation

$$\eta_A = \frac{B^2}{4\pi\gamma\rho_i\rho}, \quad (38)$$

where $1/\gamma\rho_i = \tau_{ni}$ is the neutral-ion momentum exchange timescale, parameterised as

$$\tau_{ni} = \frac{\tilde{\eta}_A}{\sqrt{4\pi G\rho}}; \quad (39)$$

the nondimensional ambipolar diffusion parameter $\tilde{\eta}_A$ is a constant of the model (simply denoted η in KK02). η_A/B^2 is then self-similarised using the scalings above to give

$$\frac{\eta'_A}{b^2} = \tilde{\eta}_A \frac{h^{3/2}}{\sigma^{3/2}}; \quad (40)$$

it is important to note that the self-similarity of the solution depends upon the relationship $\rho_i \propto \rho^{1/2}$.

For grains with radius $a = 0.1 \mu\text{m}$ in a cloud where the temperature is 10 K and the cosmic ray ionisation rate is $\xi = 10^{-17} \text{ s}^{-1}$, simulations typically assume the ion density scales as $\rho_i \propto \rho^{1/2}$ when $10^4 \lesssim n_H \lesssim 10^7 \text{ cm}^{-3}$ (Elmegreen 1979; Kamaya & Nishi 2000). This is an oversimplification, as Ciolek & Mouschovias (1998) showed that for typical cloud and grain parameters the proportionality of the ion density cannot be parameterised by a single power law exponent, but it is still a reasonable and widely-adopted approximation to the ion density in collapsing cores on scales $\gtrsim 10^3 \text{ au}$ (see e.g. Shu et al. 1987; Galli & Shu 1993a; Ciolek & Königl 1998; Contopoulos et al. 1998, KK02).

As a matter of pragmatism, a similar scaling with respect to the density and scale height is adopted for the Hall diffusion parameter, η_H . By stating that the self-similar Hall diffusion coefficient scales as

$$\frac{\eta'_H}{b} = \tilde{\eta}_H b \frac{h^{3/2}}{\sigma^{3/2}} \quad (41)$$

where $\tilde{\eta}_H$ is the constant nondimensional Hall diffusion parameter used to characterise the solutions, the ratio of the nondimensional ambipolar and Hall diffusion parameters becomes the most important factor in determining the magnetic behaviour of the similarity solutions. In truth, the Hall diffusion coefficient could be scaled with respect to the density and field strength by multiplying the nondimensional Hall parameter by any function of the similarity variable x and the fluid variables. This topic is discussed in more detail in §5, where an alternate scaling is proposed for future work on the self-similar collapse model. The scaling of η'_H given in Equation 41 is appropriate for a molecular cloud core with grains acting as the dominant positive charge characters.

For convenience the variable $w \equiv x - u$ is used to simplify the equation set. The similarity variables are then used to rewrite Equations 20–24 in self-similar form:

$$\frac{d\psi}{dx} = x b_z, \quad (42)$$

$$\frac{dm}{dx} = x \sigma, \quad (43)$$

$$(1 - w^2) \frac{1}{\sigma} \frac{d\sigma}{dx} = g + \frac{b_z}{\sigma} \left(b_{r,s} - h \frac{db_z}{dz} \right) + \frac{j^2}{x^3} + \frac{w^2}{x}, \quad (44)$$

$$\frac{dj}{dx} = \frac{1}{w} \left(j - \frac{x b_z b_{\phi,s}}{\sigma} \right), \quad (45)$$

$$\left(\frac{\sigma m_c}{x^3} - b_{r,s} \frac{db_z}{dx}\right) h^2 + (b_{r,s}^2 + b_{\phi,s}^2 + \sigma^2) h - 2\sigma = 0, \quad (46)$$

and

$$\psi - xwb_z + \tilde{\eta}_H x b_{\phi,s} b_z b h^{1/2} \sigma^{-3/2} + \tilde{\eta}_A x b_z^2 h^{1/2} \sigma^{-3/2} \left(b_{r,s} - h \frac{db_z}{dx}\right) = 0. \quad (47)$$

These equations are augmented by the self-similar definitions

$$m = xw\sigma, \quad (48)$$

$$\dot{m} = -xu\sigma, \quad (49)$$

$$\text{and } g = -\frac{m}{x^2}; \quad (50)$$

while the other magnetic field components are given by

$$b_{r,s} = \frac{\psi}{x^2} \quad (51)$$

and

$$b_{\phi,s} = -\min \left[\frac{2\alpha\psi}{x^2} \left[\frac{j}{x} - \frac{\tilde{\eta}_H h^{1/2} b}{\sigma^{3/2}} \left(b_{r,s} - h \frac{db_z}{dx} \right) \right] \right. \\ \left. \left[1 + \frac{2\alpha\tilde{\eta}_A h^{1/2} \psi b_z}{x^2 \sigma^{3/2}} \right]^{-1}; \delta b_z \right]. \quad (52)$$

These equations completely describe the collapse of the molecular cloud core into a pseudodisc and the accretion onto the central point mass (potentially through a rotationally-supported disc). These equations are the same as equations 20–32 of KK02 in the limit of $\tilde{\eta}_H = 0$, which allows direct comparisons to be made between the similarity solutions of both models.

2.2 Outer boundary conditions

The outer regions of the collapse are modelled by a set of power law relations in the similarity variable that describe a molecular cloud core contracting quasistatically under ambipolar diffusion until it has just become supercritical and a point mass forms at the centre (e.g. Shu 1977; Shu et al. 1987).

The definition of the similarity variable (Equation 26) means that the limit $x \rightarrow \infty$ corresponds both to the outer edge of the core at $r \rightarrow \infty$ and the initial conditions of the collapse as $t \rightarrow 0$. We then describe the core as a singular isothermal sphere, which has the density profile $\rho \propto r^{-2}$ (e.g. Larson 1969; Penston 1969; Whitworth & Summers 1985), so that the surface density is:

$$\Sigma(t=0) = \frac{Ac_s^2}{2\pi Gr} \quad (53)$$

where A is a constant determined by the initial accretion rate of the core. The infall velocity and accretion rate onto the core are constant and given by

$$V_r(t=0) = u_0 c_s \quad (54)$$

$$\text{and } \dot{M}(t=0) = -\frac{Au_0 c_s^3}{G}. \quad (55)$$

The numerical results of Ciolek & Königl (1998) for the collapse of a rotating magnetic core with ambipolar diffusion showed that the accretion rate at point mass formation was

$\dot{M} \simeq 5 \text{ M}_\odot \text{ Myr}^{-1}$, corresponding to a nondimensional parameter $A \simeq 3$, which also matches to observations of many cores that show $\dot{M} \in [1, 10] \text{ M}_\odot \text{ Myr}^{-1}$ (Lee et al. 2001). As the isothermal sound speed of a core at $T = 10 \text{ K}$ is equal to $c_s = 0.19 \text{ km s}^{-1}$, the nondimensional initial infall speed must be of order unity to match observations showing $V_r = 0.05\text{--}0.10 \text{ km s}^{-1}$ (Lee et al. 2001); to match the parameter of KK02 we adopt $u_0 = -1$.

The rotational velocity of the initial core is spatially-uniform and given by

$$V_\phi = v_0 c_s \quad (56)$$

where v_0 is the dimensionless rotational velocity, which can be approximated by

$$v_0 \approx \frac{A\Omega_b c_s}{\sqrt{G}B_{\text{ref}}} \quad (57)$$

using the r^{-1} dependence of the core surface density and magnetic field as in Basu (1997). The uniform background angular velocity is typically $\Omega_b = 2 \times 10^{-14} \text{ rad s}^{-1}$ (Goodman et al. 1993; Kane & Clemens 1997) and the background magnetic field is taken to be $B_{\text{ref}} = 30 \text{ } \mu\text{G}$ (Crutcher 1999), which gives $v_0 = 0.15$. This value is a factor of ten larger than that obtained in Basu (1997), however, the range of observed core velocities is $v_0 \in [0.01, 1.0]$ (Lee et al. 2001). KK02 showed that the size of the inner Keplerian disc directly corresponds to the initial rotational velocity at the core; we take $v_0 = 0.73$ to facilitate comparison with their fiducial ambipolar diffusion solution.

Finally, in the outer regions IMHD holds true, and the mass-to-flux ratio in the gas is constant. The core is just supercritical at

$$\frac{M}{\Psi} = \frac{\mu_0}{2\pi\sqrt{G}} \quad (58)$$

where μ_0 is the dimensionless mass-to-flux ratio, parameterised with respect to the critical value for support against gravity (Nakano & Nakamura 1978). A value of $\mu_0 = 2.9$ is adopted here for compatibility with KK02; this value was obtained from the numerical simulations of Ciolek & Königl (1998) and matches observations showing that cores are typically more than twice supercritical (Crutcher 1999; but see also Crutcher et al. 2009; Mouschovias & Tassis 2009). Equation 42 can then be used to show that

$$B_z = \frac{2\pi\sqrt{G}}{\mu_0} \Sigma; \quad (59)$$

this is equivalent to Equation 58, so that only one of these may be used to calculate the similarity solution.

In self-similar form the conditions at the outer boundary x_{out} take the form

$$m = Ax_{\text{out}}, \quad (60)$$

$$\sigma = \frac{A}{x_{\text{out}}}, \quad (61)$$

$$b_z = \frac{\sigma}{\mu_0} \quad (62)$$

$$\text{and } v = v_0. \quad (63)$$

2.3 Inner boundary conditions

As the variables are integrated inward from the centrifugal shock they tend towards an inner asymptotic set of

equations describing a Keplerian disc around the protostar. These relations are found analytically by assuming that the variables take the form of power laws in x and solving Equations 42–52 for the exponents as $x \rightarrow 0$, under the assumption that there is no counter-rotation. In nondimensional form this disc is described by:

$$m = m_c, \quad (64)$$

$$\dot{m} = m_c, \quad (65)$$

$$\sigma = \sigma_1 x^{-3/2} = \frac{\sqrt{2m_c f}}{2\delta\sqrt{(2\delta/f)^2 + 1}} x^{-3/2}, \quad (66)$$

$$h = h_1 x^{3/2} = \left(\frac{2}{m_c[1 + (f/2\delta)^2]} \right)^{1/2} x^{3/2}, \quad (67)$$

$$u = -\frac{m_c}{\sigma_1} x^{1/2}, \quad (68)$$

$$v = \sqrt{\frac{m_c}{x}}, \quad (69)$$

$$j = \sqrt{m_c x}, \quad (70)$$

$$\psi = \frac{4}{3} b_z x^2, \quad (71)$$

$$b_z = \frac{m_c^{3/4}}{\sqrt{2\delta}} x^{-5/4}, \quad (72)$$

$$b_{r,s} = \frac{4}{3} b_z \quad (73)$$

$$\text{and } b_{\phi,s} = -\delta b_z. \quad (74)$$

The diffusion constant f is a function of the ambipolar and Hall diffusion parameters, and is given by the equation

$$f = \frac{4}{3} \tilde{\eta}_A - \delta \tilde{\eta}_H \sqrt{\frac{25}{9} + \delta^2}; \quad (75)$$

this definition shows how the Hall term is able to counteract the ambipolar diffusion term in determining the surface density of the disc and the accretion rate onto the central protostar when the nondimensional Hall parameter $\tilde{\eta}_H$ is positive, and add to the ambipolar diffusion if the Hall parameter is negative. The characteristic diffusion parameter of the disc, f , must be positive in order to form a Keplerian disc in solutions without counter-rotation¹; this places limits on the relative sizes of the diffusion parameters.

These relations are derived elsewhere (Braiding & Wardle, in prep): to summarise, the inner accretion disc is in Keplerian rotation in the same direction as the initial core, with the centrifugal force balancing the inwards pull of gravity. The accretion rate onto the protostar is constant and low, and accretion through the disc is determined by the total amount of magnetic diffusion, which removes radial support by the magnetic field and allows the gas to fall inwards.

A second asymptotic solution also exists (KK02; Braiding & Wardle, in prep), in which the magnetic braking is so strong that most of the angular momentum is removed from the gas, which then free falls onto the protostar without forming a disc (the magnetic braking catastrophe, described in §5). Similarity solutions matching onto this solution lie beyond the scope of the present paper.

¹ As discussed in §5, the Hall effect can cause counter-rotation of the disc; however, in all of our solutions the inner Keplerian disc is rotating in the same direction as the initial core.

3 NUMERICAL METHODS

The calculation of the similarity solutions is quite complex, as many of the derivatives are large, and sonic points and shock fronts must be calculated explicitly as they are encountered by the integration routine. Furthermore, subshocks can occur downstream of the magnetic diffusion and centrifugal shocks. Such a subshock occurred downstream of the magnetic diffusion shock in the solutions of Li (1998), and although no subshocks appeared in the published solutions of KK02 they were observed in the unpublished collapse solutions discussed in that paper. Locating and integrating through these shocks requires careful monitoring of the integration and automatic intervention where necessary. The full details of the methods used to compute the similarity solutions are described in §5.1 of Braiding (2011); only an outline is provided in this work.

The problem is recast as a two-point boundary value problem in which the variables are integrated from a matching point x_m to both the inner and outer boundaries. We employ a “shooting” routine, which modifies the values of the variables at x_m in order to zero the discrepancies between the integrated variables and their expected asymptotic values at the boundaries. The matching point is located at a position $x_c < x_m < x_d$, where x_d and x_c are the positions of the magnetic diffusion and centrifugal shocks respectively, and is typically chosen just downstream of the magnetic diffusion shock at $x_m \sim 0.3$.

The values of the variables m , σ , j , ψ and b_z at x_m and the nondimensional accretion rate onto the central mass m_c are initially unknown, and a poor guess of these can cause the integration (and by extension convergence on the true solution) to fail. An acceptable initial guess of the variables is obtained by performing a simplified integration from the outer boundary to the matching point.

3.1 Initial guess at x_m

The initial guess of the variables at the matching point is estimated by performing a simplified integration in which the induction equation has been replaced by an algebraic expression for the vertical magnetic field component. We follow the derivation of KK02 here, and in the ambipolar diffusion ($\tilde{\eta}_H = 0$) limit our equations reduce to theirs.

The initial guess of m_c is estimated from the mass plateau in the region of the magnetic diffusion shock (see §4). The outer edge of this plateau occurs at $x_{pl} \approx |u_0|$ (which is something of an overestimate as $|u|$ is typically larger than x here). The outer asymptotic behaviour is only just starting to break down in this region, and so the asymptotic relations from §2.2 are substituted into Equation 48:

$$m_c \approx m_{pl} \approx 2|u_0|A. \quad (76)$$

The calculation of the similarity solutions is less sensitive to our estimate of m_c than to the values of the other variables at the matching point. Equation 76 is an acceptable first guess of the accretion rate onto the central star.

Save for during the various shock transitions where b_z changes rapidly, the inequality $b_{r,s} \gg h(db_z/dx)$ holds true everywhere in the collapsing flow; as this term is always small compared to the other terms in the induction equation it may be dropped. The magnitude of the magnetic field b

is always of order $b_z \approx b_{r,s}$, so that it may be estimated by $b \approx \sqrt{2}b_z$. The induction equation may then be written as a quadratic in b_z :

$$xh^{1/2}\sigma^{-3/2}\left(\tilde{\eta}_H\sqrt{2}b_{\phi,s} + \tilde{\eta}_Ab_{r,s}\right)b_z^2 - xwb_z + \psi = 0. \quad (77)$$

The well-separated roots provide approximations to the behaviour of b_z on either side of the magnetic diffusion shock, with the prescription

$$b_{z,low} \approx \frac{\psi\sigma}{m} \approx \frac{\sigma}{\mu_0} \quad (78)$$

applying in the large x regime where flux freezing still mostly holds true and the mass-to-flux ratio is given by its initial value $\mu = \mu_0$. This is equivalent to the initial condition for the vertical field component and although IMHD breaks down before the magnetic diffusion shock Equation 78 remains a good approximation to the field in this region.

The larger root gives the value of the vertical field component in the magnetic diffusion regime where x is small. It is approximated by dropping the constant term in Equation 77 and solving for b_z to obtain

$$b_{z,high} \approx \frac{m}{x} \left(\frac{\sigma}{h}\right)^{1/2} \left(\sqrt{2}\tilde{\eta}_Hb_{\phi,s} + \tilde{\eta}_Ab_{r,s}\right)^{-1}, \quad (79)$$

which reduces to equation 50 of KK02 in the $\tilde{\eta}_H = 0$ limit. The thickness of the disc in this region is controlled by the magnetic squeezing, so that

$$h \approx \frac{2\sigma}{b_{r,s}^2}. \quad (80)$$

The transition between the two approximations to b_z occurs at the magnetic diffusion shock, x_d , which represents a continuous increase in the magnetic field strength, and though the matter is slowed in the post-shock region, w is near-constant and $w > 1$ throughout the magnetic diffusion shock itself. The magnetic field lines are compressed by the shock, resulting in an increase in the vertical and azimuthal field as the field lines are twisted up by the slowing of the compressed gas. Conservation of flux ensures that the radial field component does not change in the shock. On the upstream side of the magnetic diffusion shock $b_{\phi,s} \approx -\delta b_{z,low}$ (as can be seen in the solutions in §4), however downstream of the shock the azimuthal magnetic field component is given by $b_{\phi,s} \approx -w\delta b_{z,low}$. In the region of the magnetic diffusion shock $b_{\phi,s}$ is then simplified into

$$b_{\phi,s} \approx -x_d\delta b_{r,s}; \quad (81)$$

as $x_d < 1$, $b_{\phi,s} < b_{r,s}$ when $\delta = 1$, justifying our omission of the azimuthal magnetic field component from the approximations to the scale height and magnetic field amplitude.

Then using these relations and the approximation that IMHD holds true in this region, Equation 79 becomes

$$b_{z,high} \approx \frac{m}{x} \left(\sqrt{2}\tilde{\eta}_A - 2\delta x_d\tilde{\eta}_H\right)^{-1}; \quad (82)$$

applying the approximation that $b_{z,high} = b_{r,s}$ gives an estimation of the magnetic diffusion shock position:

$$x_d \approx \frac{\tilde{\eta}_A}{\sqrt{2}} \left(\frac{\mu_0}{2} + \delta\tilde{\eta}_H\right)^{-1}, \quad (83)$$

which is equivalent to KK02's equation 58 in the $\tilde{\eta}_H = 0$ limit. This value of x_d is typically accurate to 20 per cent of

the true value, which is acceptable for estimating the variables at x_m .

In order to obtain the initial guess of the variables at x_m we integrate Equations 42–46 inwards from the outer boundary, using Equation 78 to approximate b_z when $x > x_d$, and Equation 79 for $x_m < x < x_d$. These are used to integrate the full set of equations in both directions from x_m ; the deviation of the results from the expected asymptotic boundary conditions is minimized by the shooting routine, which tweaks the variables at x_m to reduce the discrepancies. Once the initial values at x_m are close to the true solution the shooting routine will converge quadratically.

Integration of the full equation set in the outwards direction is usually performed without difficulty unless a particularly poor guess of the variables at x_m is employed. The magnetic diffusion shock is continuous and may be integrated through without pause. As magnetic diffusion is not important in this region the integration to the boundary (typically located at $x_{out} = 10^4$ – 10^5) is rapid and uncomplicated. Integrating in the inwards direction is more problematic as the calculation is very sensitive both to the values of the variables at x_m and the Hall diffusion parameter.

3.2 Inwards integration to x_c

Integrating inwards is complicated by the presence of shock discontinuities and sonic points, which must be calculated explicitly. Close to the magnetic diffusion shock there may occur a subshock in which the supersonic (but slowing due to the sudden increase in b_z) inflow is abruptly slowed to a subsonic rate. This only occurs when the Hall parameter is positive, and is likely caused by the changed magnetic braking triggered by the azimuthal field growth during the shock. This subshock is a sharpening of the post-shock variation of the density and infall speed in the solutions of KK02.

The magnetic diffusion subshock's existence is detected by performing a test integration: if the variables approach a sonic point (where $w^2 = 1$) then a shock must exist upstream. Its position is found using the same method as that for the centrifugal shock described below, using the same jump conditions. Downstream of this subshock a sonic point occurs as the radial velocity becomes supersonic once more; a small manual step through the sonic point is performed and the variables are integrated to the centrifugal shock.

The position of the centrifugal shock is found by performing a binary search over an appropriate interval. The upper and lower bounds on x_c are described by $x_{c0} \pm 0.2x_{c0}$ where x_{c0} is estimated from KK02's equation 65, using $(\tilde{\eta}_A - \delta\tilde{\eta}_H)$ in place of $\tilde{\eta}_A$:

$$x_{c0} \approx \frac{v_0^2}{A^2} m_c \exp \left[-\sqrt{\frac{2^{3/2}m_c}{\mu_0(\tilde{\eta}_A - \delta\tilde{\eta}_H)^3}} \right]. \quad (84)$$

This is an overestimate of the true shock position (typically by around 20 per cent), however the routine is sufficiently robust that this does not present a problem. The variables are integrated to the estimated position of x_{c0} , where the jump conditions derived below are applied, and then integrated towards the inner boundary. Unless the shock position is known very precisely, the variables will approach their asymptotic values and then veer off course.

This behaviour is most clearly seen in the surface den-

sity σ , which increases rapidly downstream of the shock if x_{c0} is an overestimate to the true shock position, and drops dramatically if x_{c0} is an underestimate. The incorrect estimate is then assigned to be the new boundary of the shock position as appropriate, and a new estimate of x_{c0} is chosen at the midpoint between the boundaries. As the position of the shock is more precisely known, the variables follow the asymptotic behaviour longer.

The potential presence of any sonic points and subshocks does not interfere with the iterative routine for finding the shock position. When there exists a sonic point downstream of the shock: σ bounces upwards at the sonic point if x_{c0} is too high, while if x_{c0} is too low then the integration fails at the sonic point. When the shock position is known to approximately 10^{-10} , it is considered to be known to the precision of the full calculation.

The variables are integrated inwards from the centrifugal shock and if $\tilde{\eta}_H$ is large enough they are manually integrated through the sonic point that presages the existence of a centrifugal subshock. After the sonic point, the binary search is employed again to find the position of its associated shock front, as the behaviour of the variables downstream of the subshock is unchanged. In this instance the initial upper boundary of the search (x_{up}) is the sonic point, and the lower boundary is $x_{down} = 0.1x_{up}$. If $\tilde{\eta}_H$ is so large that multiple subshocks exist then this behaviour repeats, with the first subshock followed by an additional sonic point and then a second subshock; the increasing number of subshocks cause the calculation to become so unstable that it is unable to converge on the true similarity solution.

Note that even when the shock positions are known “precisely”, the routine is often unable to complete the integration all the way to the inner boundary. This is avoided by integrating a simplified set of equations from a point far from the centrifugal shock to the inner boundary. These equations and the matching criteria are outlined in §3.4.

3.3 Jump conditions

The magnetic diffusion shock is smooth and continuous, and does not require any explicit calculation of shock conditions. The shock is the transition between the approximations $b_{z,low}$ and $b_{z,high}$ (Equations 78 and 79), and in the shock front b_z , $b_{\phi,s}$ and h are changed, with $b_{\phi,s}$ downstream of the shock given by $b_{\phi,s} \approx -wx_d\delta b_{z,low}$. During the shock the scale height is markedly compressed, suggesting that a breakdown of vertical hydrostatic equilibrium has occurred. In reality the enhanced magnetic squeezing during the shock front would be unable to reduce the disc thickness so dramatically over the fluid transit time through the shock, which implies that the thinness of the compressed region is a numerical artefact. Furthermore, as the magnetic pressure far exceeds the gas pressure any breakdown of isothermality would not greatly affect the collapse.

The centrifugal shock is a true discontinuity in the fluid variables, which must be explicitly calculated. The shock conditions used are those for the “isothermal jump” in KK02; these are found by recognising that the derivatives of the surface density and radial velocity at the shock are large compared to the other terms in the conservation of mass and radial momentum equations (43 and 44). The equations are

integrated over the shock to give the relations

$$\sigma w = \text{constant} \quad (85)$$

$$\text{and } \sigma(w^2 + 1) = \text{constant}, \quad (86)$$

which apply when the magnetic forces are small. These equations give the non-trivial jump conditions:

$$w_d = \frac{1}{w_u} \quad (87)$$

$$\text{and } \sigma_d = \sigma_u w_u^2, \quad (88)$$

where u and d denote the upstream and downstream sides of the shock; these are also used for any subshocks downstream of the principal shocks. KK02 also derived jump conditions for use when the magnetic forces are important; these are not required in this work. It is possible that as the positive Hall parameter becomes larger the magnetic diffusion subshock may require different jump conditions that take the twisting of the magnetic field lines due to the Hall effect into account.

The magnetic field strength does not change in the centrifugal shock front as the magnetic pressure and tension terms are not large enough to change the field behaviour. In the post-shock region the field increases as the other variables settle to the asymptotic behaviour in §2.3. While the magnetic field is unchanged by the passage of the shock, its position and strength depend upon the Hall parameter. The increased magnetic diffusion can also cause the formation of subshocks – rings of sharply-enhanced density in the post-shock region – as the outward-moving flux causes the infalling gas to be slowed.

As with the magnetic diffusion subshock, the centrifugal subshocks are preceded by a sonic point that must be calculated manually and the subshock position is found using the binary search above. Inwards of the centrifugal shocks the variables approach the asymptotic behaviour with some overshoots and corrections.

3.4 Innermost integration

In the innermost regions of the collapse the derivatives $d\sigma/dx$ and db_z/dx become very large in comparison to the other derivatives. These can correspondingly cause small numerical errors in the calculation of these derivatives and their integrals to build and trigger the appearance of a spontaneous singularity where the variables diverge dramatically from the asymptotic solution (discussed in Li 1998). This behaviour is avoided by replacing the full MHD equations with a simplified set that can be integrated all the way to the inner boundary: the problematic derivatives are replaced by approximations derived from the expected asymptotic behaviour, that is,

$$\frac{db_z}{dx} = -\frac{5}{4} \frac{m_c^{3/4}}{\sqrt{2\delta}} x^{-9/4} \quad (89)$$

$$\text{and } \frac{d\sigma}{dx} = -\frac{3}{2} \frac{\sqrt{2m_c f}}{2\delta\sqrt{(2\delta/f)^2 + 1}} x^{-5/2}. \quad (90)$$

These are then substituted into the other equations so that σ , b_z , $b_{\phi,s}$ and h are found by solving Equations 44, 46, 47 and 52 simultaneously, while the remaining equations are integrated to the boundary.

Switching between the full and simplified models occurs

Table 1. Boundary conditions and parameters.

| parameter | | value |
|---------------------|------------------|-------|
| ambipolar diffusion | $\tilde{\eta}_A$ | 1.00 |
| cap on $b_{\phi,s}$ | δ | 1.00 |
| magnetic braking | α | 0.08 |
| boundary condition | | value |
| mass-to-flux ratio | μ_0 | 2.90 |
| rotational velocity | v_0 | 0.73 |
| radial velocity | u_0 | -1.00 |
| core accretion rate | A | 3.00 |

after the minimum in the surface density as the variables follow the asymptotic solution, but before they diverge from the expected behaviour. Typically this occurs when the old and new values of σ match to within $0.01/x$ (~ 0.1 per cent of the original value) and $d\sigma/dx$ calculated using both methods matches less well to around $200/x$ (~ 7 per cent). When the precision of the match is as high as possible the change between the two equation sets is smooth; the required precision of the match is raised when the switch is apparent as this clearly influences the accuracy of the calculations.

The simplified set of equations is not subject to the same numerical instabilities as the full set unless the guess at the matching point is particularly poor. Should such a guess be adopted then the routine is unable to match onto the simplified model, and the failure of the inwards integration is used to refine the values at the matching point.

The integration is continued to the inner boundary (typically at $x_{\text{in}} = 10^{-4}$) where the variables are compared to the inner conditions given by Equations 64 and 71. The differences between the expected and integrated variables are passed back to the shooting routine, which modifies the values at x_m and begins the next iteration. The similarity solution is considered to have converged when the integrated variables match the boundary conditions to at least 0.002 per cent. Due to the ease of convergence in the outwards direction, the outer variables match to a much higher degree.

4 RESULTS

Superficially, the similarity solutions with Hall diffusion are similar to the fiducial ambipolar diffusion solution of KK02. We match their boundary conditions and parameters, listed in Table 1, holding the ambipolar diffusion parameter constant at $\tilde{\eta}_A = 1.0$ so that the only changes between the similarity solutions presented in their work and ours are those wrought by the addition of Hall diffusion.

4.1 Ambipolar diffusion solution

As a test of the computational code we calculate the fiducial ambipolar diffusion solution of KK02 in Fig. 1, and follow their discussion of the solution here. The outer regions of all the solutions match IMHD similarity solutions, as the mass-to-flux and mass-to-angular momentum ratios are constant while the material falls in at supersonic speeds. The radial velocity and scale height are dominated by the self-gravity of

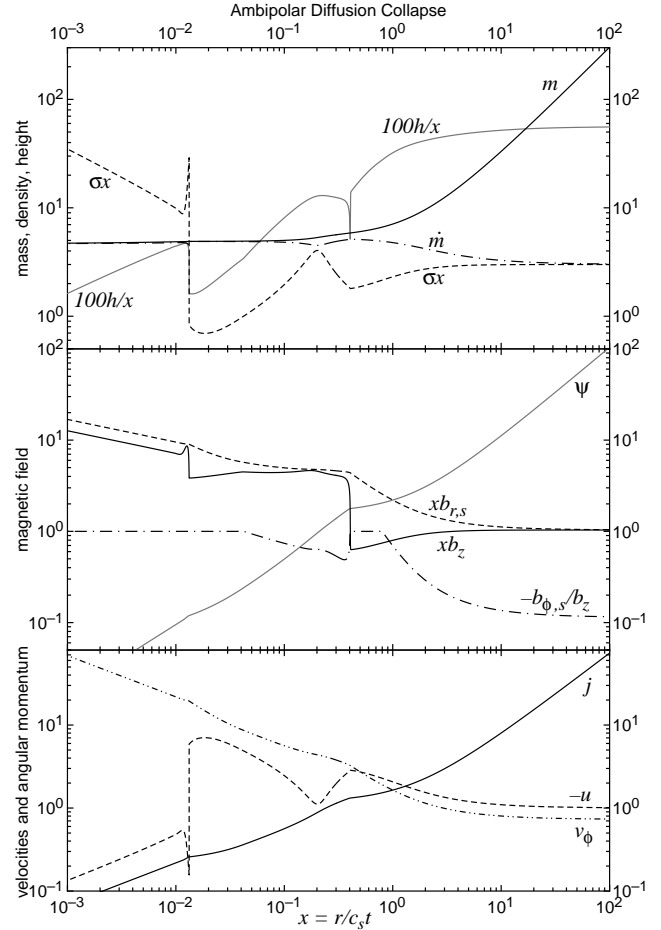


Figure 1. Calculated similarity solution for collapse with only ambipolar diffusion, duplicating KK02's fig. 7. The enclosed mass, accretion rate, surface density and scale height are displayed in the upper panel; the magnetic field components and enclosed flux in the centre panel; and the gas velocities and angular momentum in the lower panel. The parameters and boundary conditions are as in Table 1; the central mass is $m_c = 4.67$; and the magnetic diffusion and centrifugal shocks are located at $x_d = 0.406$ and $x_c = 1.32 \times 10^{-2}$ respectively.

the disc, which causes the material to fall towards the mid-plane before it is accelerated towards the central mass. The magnetic field gradually builds up as the matter falls inward, becoming important to the dynamics at around $x \approx 2$ where magnetic braking starts to affect the angular momentum transport and the constant ratio of the mass-to-angular momentum breaks down. The azimuthal field attains its capped value, and becomes important to the angular momentum transport.

The mass and angular momentum in this region tend towards plateau values: the mass to that in Equation 76, and the angular momentum to

$$j_{pl} \approx \frac{m_{pl} v_0}{A}, \quad (91)$$

which depends upon the boundary conditions. This plateau forms as the gravity of the central point mass starts to dominate and the gas starts to fall inward rapidly. The surface density and magnetic field build up and ambipolar diffusion

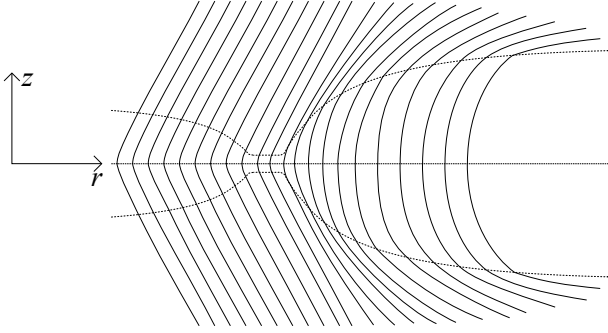


Figure 2. Schematic of the poloidal magnetic field in the magnetic diffusion shock. The disc (dotted lines) is compressed as the vertical field becomes large, causing the field lines at the surface to straighten from being largely radial upstream to having roughly equal poloidal components downstream. (Not to scale.)

becomes important, causing flux-freezing to break down at the magnetic diffusion shock (at $x_d = 0.406$).

This shock takes the form of a sudden increase in the vertical magnetic field as the field lines diffusing against the flow in the downstream ambipolar diffusion-dominated regime meet those coming inward under IMHD collapse. The field geometry is illustrated in Fig. 2: upstream the surface magnetic field is dominated by the radial component, which is an order of magnitude larger than the vertical and azimuthal components. During the shock (and the downstream transition region) the field lines straighten until the poloidal components are approximately equal at the disc surface. The increase in field strength slows the gas, and magnetic squeezing comes to dominate the vertical compression.

Immediately interior to the magnetic diffusion shock the poloidal field components scale with $\sim x^{-1}$ as the surface density and thickness of the disc increase and the gas is slowed by the radial magnetic pressure. Rotation is not dynamically important and the shock has a similar structure to that in the nonrotating similarity solutions of Contopoulos et al. (1998). The gravity of the central mass becomes the dominant radial force on the gas at the end of the post-shock region (the peak in the surface density) and the matter is accelerated inwards until it is in near-free fall collapse.

As in slowly-rotating similarity solutions that are non-magnetic (e.g. Saigo & Hanawa 1998) or include IMHD (e.g. KK02 §3.2) rotation remains dynamically unimportant until the vicinity of the centrifugal shock. Between the two shocks the gravity of the central mass dominates the radial infall of the gas, which is slowed only a little by ambipolar diffusion of the magnetic flux and the magnetic pressure. The magnetic braking increases the azimuthal field component until it is again capped; the activation of the cap causes the change in the behaviour of the scale height at $x \sim 4.5 \times 10^{-2}$ as $b_{\phi,s}$ then contributes more to the vertical squeezing forces. The enclosed mass and accretion rate flatten and remain near-constant throughout the remainder of the collapse. The angular momentum starts to plateau again and the centrifugal force becomes large and equal to the gravitational force, triggering the centrifugal shock at $x_c = 1.32 \times 10^{-2}$.

The centrifugal shock slows the gas so that the infall is subsonic and the surface density increases by more than an

order of magnitude. The shock is followed by a thin layer in which the azimuthal and vertical magnetic field components increase rapidly. This causes the angular momentum to drop to its asymptotic behaviour, as the surface density and the other variables adjust with a few overshoots towards their expected rotationally-supported disc behaviour. The transition between the full model and the simplified set of equations occurs at $x \sim 8.6 \times 10^{-3}$, after the variables have joined onto the asymptotic disc described by Equations 64–74.

The Keplerian disc itself is small, with a mass ~ 5 per cent that of the central point mass. The nondimensional mass at the origin is $m_c = 4.67$, corresponding to a moderate accretion rate of $\dot{M}_c = 7.6 \times 10^{-6} M_\odot \text{ yr}^{-1}$ (so that at a time $t = 10^5 \text{ yr}$, the central mass is $M_c = 0.76 M_\odot$). The surface density of the disc depends upon the ambipolar diffusion and azimuthal field cap parameters, as does the infall velocity, which is subsonic and very low. The disc is extremely thin, and the vertical squeezing is dominated by the tidal and self-gravitational forces. The magnetic flux in the disc scales as $x^{3/4}$, so that $\psi \rightarrow 0$ as $x \rightarrow 0$; clearly the amount of flux present in the protostar depends upon more detailed flux transport and destruction mechanisms than are included in this model, such as Ohmic diffusion (e.g. Li & McKee 1996) and reconnection (e.g. Galli & Shu 1993b; Lazarian 2005).

4.2 Hall diffusion solutions

The first of the similarity solutions with Hall diffusion is that presented in Fig. 3 for the self-similar collapse of a molecular cloud with $\tilde{\eta}_H = -0.2$ and other parameters matching those in Fig. 1. The negative Hall parameter solutions have more radial diffusion of the magnetic field against the neutral fluid and charged grains, so that the magnetic pressure builds up earlier in the collapse process, triggering the formation of the magnetic diffusion shock. The negative Hall parameter also increases the initial rate of magnetic braking so that $b_{\phi,s}$ attains its capped value earlier in the collapse, and the magnetic braking is then determined by the strength of the vertical field component.

As in the no-Hall solution, at the outer edge of the collapse in Fig. 3 the matter is falling in supersonically under IMHD. As the surface density builds up the field does too, causing the magnetic pressure and tension terms to become important, while the magnetic braking transports angular momentum from the infalling gas to the external envelope. The angular momentum and enclosed mass start to plateau as the dominant force on the radial velocity switches from the self-gravity of the disc to the gravity of the central mass, which in turn causes the accretion rate to taper off. The formation of the magnetic diffusion shock at $x_d = 0.461$ (increased from the non-Hall solution) is caused by the decoupling of the field from the neutral particles.

The magnetic diffusion shock in this solution is weaker than in Fig. 1 as most of the neutral particles and grains have already decoupled from the magnetic field, so that the vertical field component increases by only 4.5 times (*cf.* 6.2 times in Fig. 1). The disc is less vertically compressed by the field, producing a thinner shock, and $b_{\phi,s}$ does not grow as rapidly. Within the shock the field is further decoupled from the neutrals and grains, allowing Hall and ambipolar diffusion to become more important downstream of the shock and throughout the remainder of the solution. The field lines

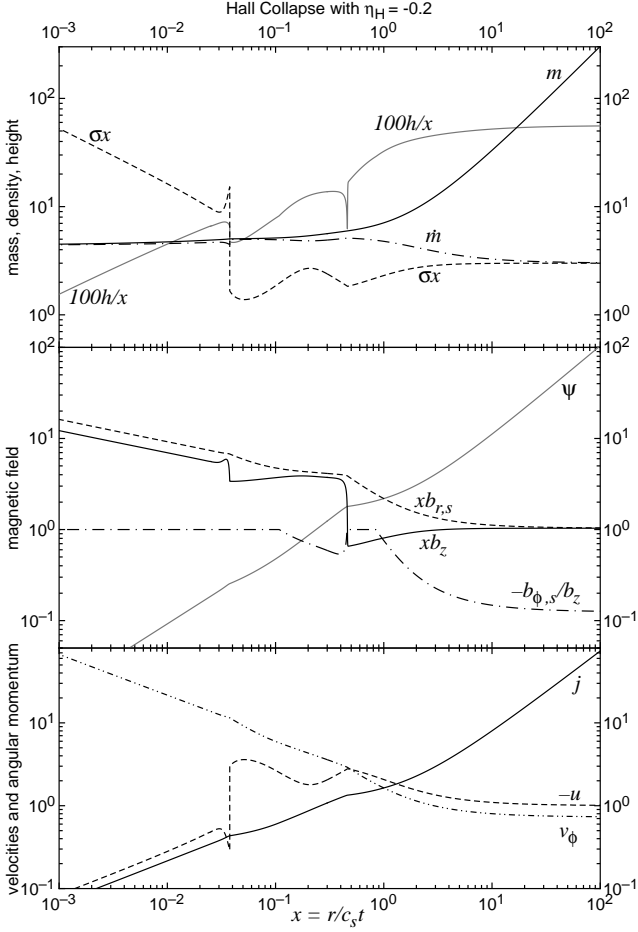


Figure 3. Hall collapse with $\tilde{\eta}_H = -0.2$. The variables are as in Fig. 1; the parameters and boundary conditions are given in Table 1. The central mass is $m_c = 4.23$; the magnetic diffusion and centrifugal shocks are located at $x_d = 0.461$ and $x_c = 3.78 \times 10^{-2}$ respectively; these are increased from the non-Hall positions, and the post-shock regions are smoothed by Hall diffusion.

straighten as in Fig. 2; although the radial field component is still dominant, the vertical component increases in the shock until it is just smaller than $b_{r,s}$.

Downstream of the magnetic diffusion shock the surface density gradually increases as the infall velocity is slowed by the larger magnetic support. This post-shock region is smoother than that without Hall diffusion, presenting a gentler transition to the free fall collapse that occurs outside of the rotationally-supported disc. The vertical field scales as x^{-1} in this region as the increased radial diffusion means that there are fewer field lines in total moving against the flow of the neutral particles. The magnetic braking decreases the angular momentum efficiently until $b_{\phi,s}$ attains its capped value and j begins to plateau once more.

The centrifugal force builds up and triggers the centrifugal shock at $x_c = 3.78 \times 10^{-2}$ (cf. $x_c = 1.32 \times 10^{-2}$ in Fig. 1). The shock is a discontinuity in the surface density and radial velocity, which is again less strong than in the solution without Hall diffusion, and inwards of this the vertical and azimuthal field components increase steeply as the field reacts to the shock (although $b_{\phi,s}$ remains capped

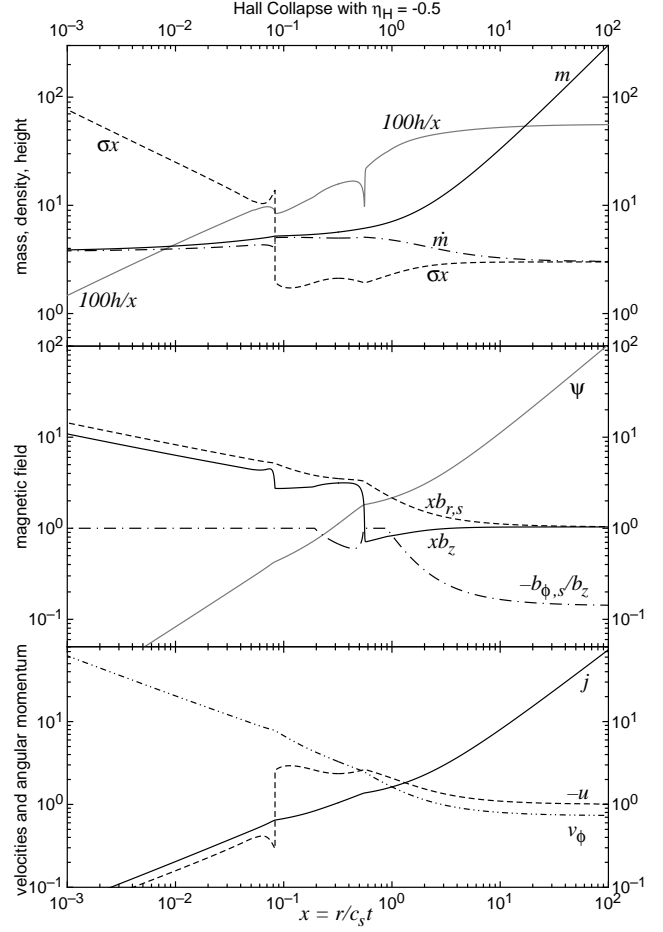


Figure 4. Collapse with larger Hall parameter $\tilde{\eta}_H = -0.5$. The boundary conditions and parameters match those in Fig. 3 (Table 1). The central mass is reduced to $m_c = 3.77$ and the magnetic diffusion and centrifugal shocks moved outwards to $x_d = 0.557$ and $x_c = 8.31 \times 10^{-2}$ as the increased magnetic diffusion smooths the post-shock regions and increases the size of the Keplerian disc.

at $-\delta b_z$). Downstream the variables tend (with overshoots) towards their asymptotic values.

The inner disc is in Keplerian rotation satisfying Equations 64–75. The central mass is $m_c = 4.42$, decreased from the non-Hall solution, and corresponds to an accretion rate of $\dot{M}_c = 7.21 \times 10^{-6} M_\odot \text{ yr}^{-1}$. The scalings of the other variables with respect to x are the same as in Fig. 1, however the surface density is increased by the larger magnetic diffusion parameter $f = 1.72$ (cf. $f(\tilde{\eta}_H = 0) = 1.3$); and the increased radial magnetic diffusion causes the strength of the magnetic field to be decreased from that in the ambipolar diffusion-only solution. This in turn means that less matter can lose its angular momentum and fall onto the central mass, so that the gas is at a higher surface density in this larger Keplerian disc.

The next similarity solution, presented in Fig. 4, shows the calculation with $\tilde{\eta}_H = -0.5$ on the same scale and with the same parameters as Fig. 3. The total radial magnetic diffusion is further increased so that many of the neutral particles have decoupled from the field before the magnetic diffusion shock at $x_d = 0.557$; this causes the intensity of the shock to drop further so that the vertical field strength

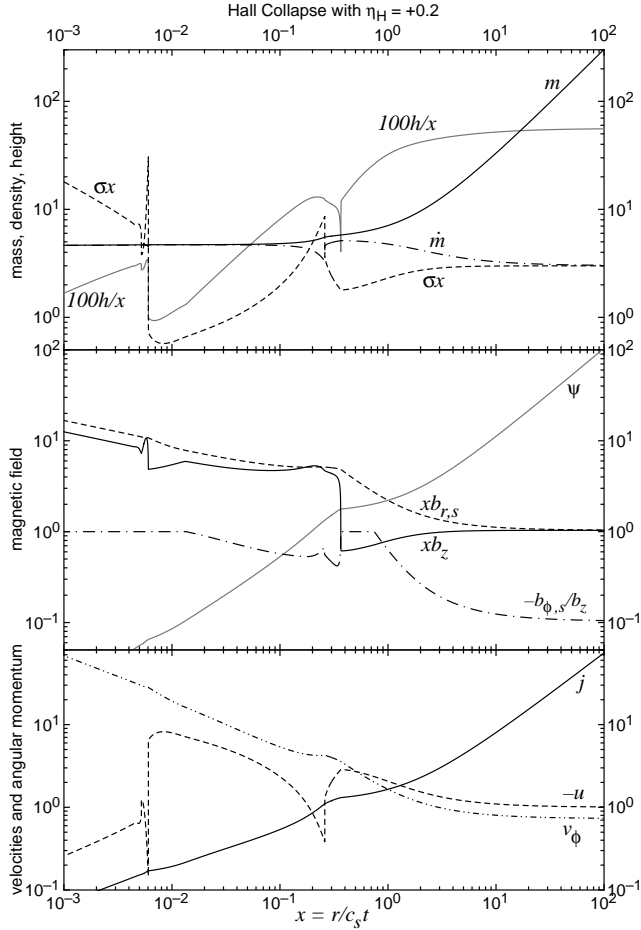


Figure 5. Gravitational collapse with positive Hall parameter $\tilde{\eta}_H = +0.2$. The boundary conditions and parameters match Fig. 3 and Table 1; the central mass is $m_c = 4.63$. The positive Hall term causes the formation of subshocks: the magnetic diffusion shocks are located at $x_d = 0.365$ and $x_{d2} = 0.260$; the centrifugal shocks at $x_c = 6.05 \times 10^{-3}$ and $x_{c2} = 5.21 \times 10^{-3}$.

is only 4 times larger than its original value. There is less of a magnetic wall at this point as less flux remains to be decoupled from the neutrals within the shock itself.

As in the previous solution with negative Hall parameter the post-magnetic diffusion shock region is smoothed, with even less change in the surface density and radial velocity. The gas is slowed by the magnetic diffusion shock, but the gravity of the central mass quickly overcomes this and pulls the fluid inwards. The radial velocity downstream of the post-shock region increases as the fluid nears the protostar, however it remains below the free fall velocity at all times. The mass and angular momentum both plateau in this region before the increasing centrifugal force triggers the centrifugal shock.

The centrifugal shock occurs much earlier in this similarity solution at $x_c = 8.31 \times 10^{-2}$. This is brought about by the decreased values of b_z and $b_{\phi,s}$ in the free fall region, which reduce the amount of magnetic braking that takes place and cause the centrifugal force to become important earlier. Inwards of this shock is a much wider region of adjustment as the variables join the inner disc solution.

The Keplerian disc is substantially larger than that in

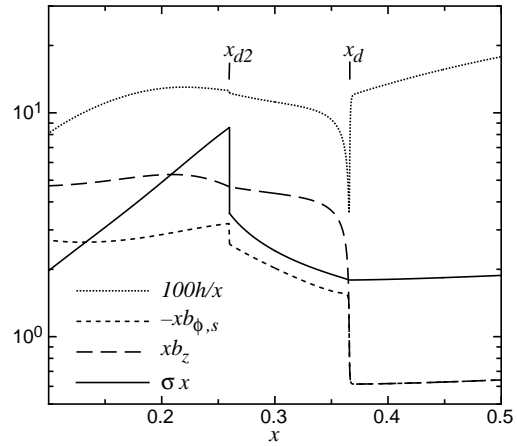


Figure 6. The magnetic diffusion shock and subshock x_{d2} , for the collapse with $\tilde{\eta}_H = +0.2$. As seen in Fig. 5, j and v_ϕ are continuous, and $-u$ mirrors the behaviour of σx .

the previous solution, containing ~ 38 per cent of the mass of the central protostar. The surface density has also increased as the magnetic diffusion parameter is $f = 2.31$, while the lowered central mass $m_c = 3.77$ corresponds to a central accretion rate of $\dot{M}_c = 6.15 \times 10^{-6} M_\odot \text{ yr}^{-1}$. Again, the larger disc corresponds to a lower accretion rate, as the reduced magnetic braking prevents the fluid from losing rotational support and falling in.

The final solution presented here is that with $\tilde{\eta}_H = +0.2$ in Fig. 5, which is the most dynamically different from those of KK02. Although the initial conditions and parameters match those in Fig. 3, the change in the sign of the Hall parameter, which corresponds to a reversal of the orientation of the magnetic field with respect to the direction of rotation, introduces many changes to the collapse dynamics.

These begin at the magnetic diffusion shock, which has moved inwards from $\tilde{\eta}_H = 0$ solution to $x_d = 0.366$. This shock is of increased intensity due to the reduced radial magnetic diffusion upstream, which causes a larger increase in b_z in the shock. The magnetic braking downstream is increased by the presence of a stronger field and the sign of the Hall term in Equation 52. The disc is more sharply compressed as the field lines straighten at the shock front, and the fluid is so slowed by the increase in the magnetic pressure that a second shock front forms at $x_{d2} = 0.260$.

In the magnetic diffusion subshock, shown at higher resolution in Fig. 6, the fluid is slowed until the radial velocity is low and subsonic. The surface density increases under the jump conditions from §3.3; this ring of matter contains approximately 18 per cent of the protostellar mass. The azimuthal field component and the scale height also increase, while db_z/dx decreases steeply. The infall region downstream of the subshock is wider in logarithmic similarity space than in the previous solutions, with the increased magnetic braking reducing the angular momentum more quickly as the radial velocity increases. The surface density drops as the fluid falls in and magnetic squeezing dominates the vertical compression until the gravity of the central mass takes over near the centrifugal shock.

The centrifugal shock occurs at $x_c = 6.05 \times 10^{-3}$, half that of the $\tilde{\eta}_H = 0$ solution, dramatically decreasing the size

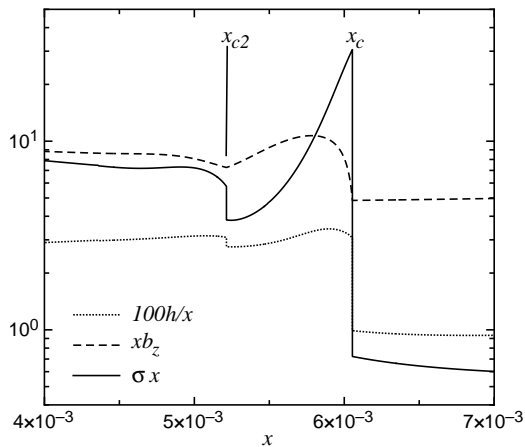


Figure 7. The centrifugal shock and subshock (denoted x_{c2}), for the $\tilde{\eta}_H = +0.2$ solution on a linear x scale. Again, j and v_ϕ are continuous, while $-u$ mirrors σx as in Fig. 5.

of the rotationally-supported disc. This change is brought about by the increased magnetic braking caused by the positive Hall parameter, which reduces the angular momentum so that the centrifugal force is not dynamically important until the gas is very close to the protostar. Downstream of the shock the slowed fluid accelerates inwards as the magnetic field increase forces additional magnetic braking and a drop in the centrifugal force. The surface density drops as the infall velocity becomes supersonic, and the centrifugal force becomes important once more, triggering the subshock at $x_{c2} = 5.21 \times 10^{-3}$ which is shown in Fig. 7. The matter is slowed in the subshock until it is again subsonic. Although the surface density increases in the subshock, the disc does not become gravitationally-unstable as the Toomre Q parameter (Toomre 1964) remains above 8 in this region.

Downstream of the subshock the variables again settle with overshoots to the Keplerian disc behaviour. The central mass is $m_c = 4.63$, corresponding to a protostellar accretion rate of $\dot{M}_c = 7.53 \times 10^{-6} M_\odot \text{ yr}^{-1}$, while the disc contains only 1.6 per cent the protostellar mass. The magnetic diffusion parameter is $f = 0.945$, reflecting the decrease in surface density as the magnetic field strength increased.

The magnetic diffusion and centrifugal subshocks both occur only in the calculations where $\tilde{\eta}_H$ is positive, as the larger magnetic pressures and braking caused by the increase in the infalling magnetic field force the gas to rapidly change in radial velocity and density. The number of centrifugal subshocks increases with $\tilde{\eta}_H$ — three subshocks have been observed in one similarity solution that was not properly converged (due to the numerical instability of the subshocks) at the time of publication — while only one magnetic diffusion subshock has been observed.

The diffusion parameter of the disc, f , cannot be less than or equal to zero in our collapse solutions, which do not contain counter-rotation. This restriction limits the range of positive $\tilde{\eta}_H$ that can be explored: as $\tilde{\eta}_H$ increases, the size and surface density of the rotationally-supported disc decrease, and the rings of gas formed by the subshocks are more likely to be gravitationally unstable. Similar constraints were found to limit the launching of disc winds in the analysis of Salmeron et al. (2011), who showed that disc

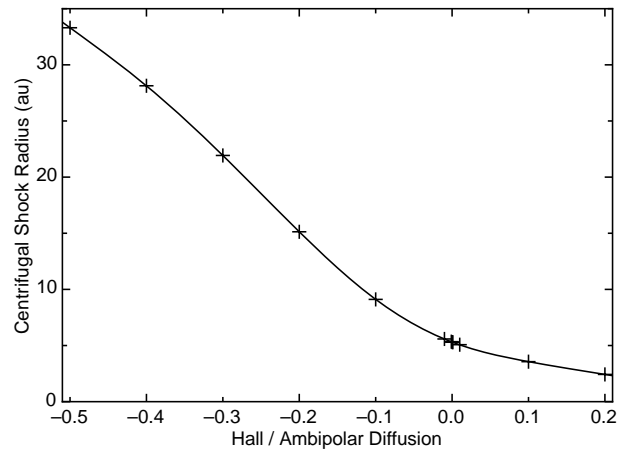


Figure 8. The centrifugal shock radius (in au at 10^4 years) against the ratio of the Hall to ambipolar diffusion parameters.

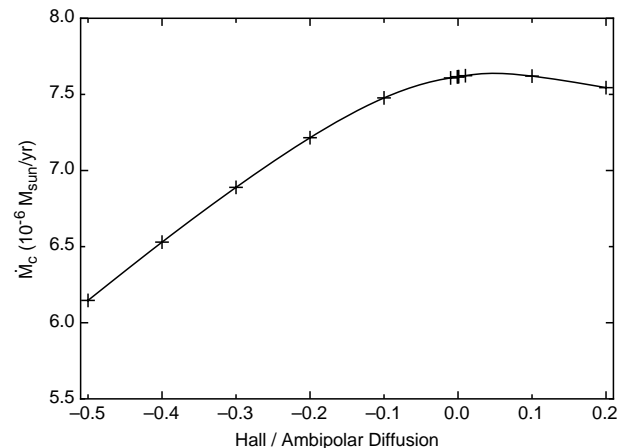


Figure 9. The protostellar accretion rate (in $10^{-6} M_\odot/\text{yr}$) against the ratio of the Hall to ambipolar diffusion parameters.

wind solutions only exist for particular combinations of the field polarity and the ratio of the Hall to ambipolar diffusion parameters.

The positions of the shocks change with the Hall parameter as demonstrated in Fig. 8, which plots the dimensional centrifugal shock position for similarity solutions with parameters as in Table 1 at 10^4 years (illustrated in Braiding 2011) against the ratio of the Hall to ambipolar diffusion parameters. While both directions of Hall drift contribute to the size of the disc, the radial drift of B_z (which increases when $\tilde{\eta}_H < 0$) has a greater effect on the radius of the centrifugal shock than the azimuthal Hall drift.

There also exists a correlation between the accretion rate onto the central protostar and the radial magnetic field diffusion, shown in Fig. 9 (see also Contopoulos et al. 1998). The accretion depends upon the disc radius, with larger discs corresponding to lower accretion rates and vice versa (Allen et al. 2003b), as a more negative Hall parameter causes increased drag on the neutrals and reduces the radial velocity of the fluid. The disc radius also depends on the initial rotational velocity, as the centrifugal force is more

important and a larger disc forms when the initial angular momentum of the core is large (KK02).

The protostellar accretion rate appears to turn over at around $\dot{M}_c = 7.6 \times 10^{-6} \text{ M}_\odot \text{ yr}^{-1}$ as the ratio of the Hall to ambipolar diffusion parameters becomes positive and greater than 0.05. This is due to the formation of subshocks in the solutions with $\tilde{\eta}_H > 0$: as the density is enhanced accretion through the disc drops. As the Hall parameter increases further subshocks are introduced, the diffusion parameter tends towards zero and the rings formed by the subshocks become more unstable.

5 DISCUSSION

The similarity solutions clearly show that Hall diffusion changes the structure and dynamics of the collapse of molecular cloud cores into protostars and protostellar discs. The rotationally-supported disc size, and the accretion rate onto the protostar are determined by the ratio of the Hall and ambipolar diffusivities, which influences the magnetic braking affecting the rotation of the collapsing core. It is also clear that Hall diffusion can inhibit disc formation by enhancing the magnetic braking, or by counteracting ambipolar diffusion to the point that the field starts to infall faster than the fluid, increasing the magnetic pressure and tension.

The dependence of the similarity solutions on the orientation of the magnetic field and the sign of the Hall diffusion parameter $\tilde{\eta}_H$ (more specifically upon the sign of $\tilde{\eta}_H(\mathbf{B} \cdot \boldsymbol{\Omega})$) gives rise to two different patterns of collapse behaviours. The similarity solutions with $\tilde{\eta}_H = 0$ and ± 0.2 are converted to dimensional form and plotted against the radius r (at $t = 10^4$ years) in Fig. 10, with the surface density in the upper panel and the vertical magnetic field strength plotted as rB_z in the lower. The solutions have the same boundary conditions and parameters (Table 1), and the surface density and vertical field strength (at $r = 1$ au), the central mass, and the mass and size of the inner disc (all at $t = 10^4$ years) are listed in Table 2. The outer regions where IMHD holds are near-identical and it is only near the magnetic diffusion shock at $r \approx 100$ au that the changes brought on by Hall diffusion become apparent.

The dotted lines in Fig. 10, corresponding to the negative Hall solution in Fig. 3, show the formation of a large rotationally-supported disc that has radius $R_c \approx 15$ au at ($t = 10^4$ years) and the highest inner Keplerian disc surface density of all the solutions. The dashed lines are the $\tilde{\eta}_H = 0$ solution from Fig. 1, which possesses a disc radius half that the negative Hall solution. The surface density of the Keplerian disc has decreased by a constant factor from that in the negative Hall solution. Finally, the solid curves characterise the similarity solution with positive Hall parameter $\tilde{\eta}_H = 0.2$ (Fig. 5) which has a Keplerian disc that is almost an order of magnitude smaller than that in the negative Hall case. This disc is bounded by a thin ring of enhanced density that rapidly drops off as the magnetic field peaks; the material is then shocked again and comes to match onto the inner solution. The density is much lower than in previous solutions, and the disc grows at a slower rate.

The similarity solutions span many orders of magnitude in both radius and density, and the inclusion of a Hall parameter that is 20 per cent that of the ambipolar diffusion

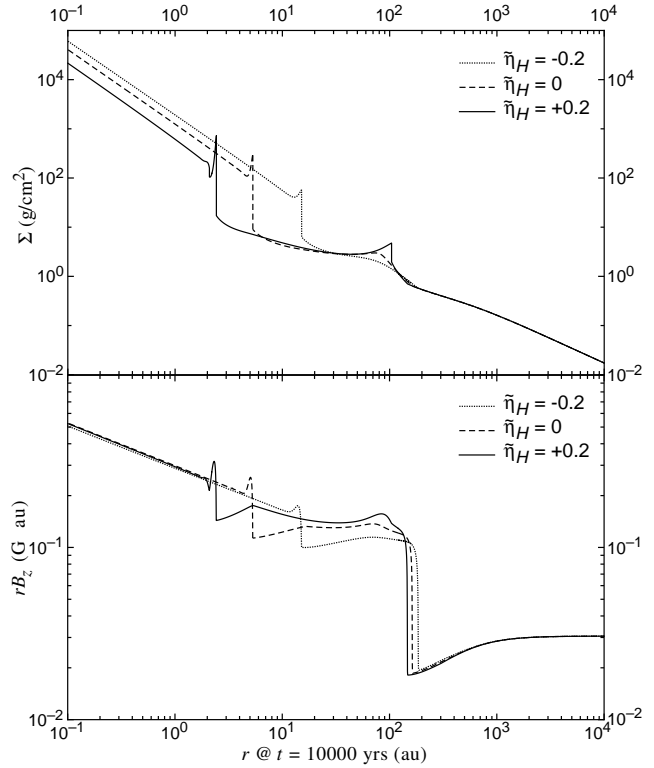


Figure 10. The surface density Σ and the vertical magnetic field component B_z plotted against radius at $t = 10^4$ yr for the solutions with $\tilde{\eta}_A = 1.0$ and $\tilde{\eta}_H = -0.2$ (dotted line), 0 (dashed line) and $+0.2$ (solid line). These solutions were plotted individually in nondimensional form in Figs. 3, 1 and 5 respectively.

parameter has a large effect on the behaviour of the magnetic field. In the intermediate region between the magnetic diffusion shock (at $R_d \approx 100$ au in Fig. 10) and the centrifugal shock ($R_c \approx 1-10$ au), the azimuthal field tension causes the Hall drift to enhance the radial diffusion of the field lines when $\tilde{\eta}_H$ is negative. The magnetic diffusion shock occurs earlier in the collapse and is less dynamic than in the other solutions, as much of the field has already been decoupled from the fluid.

However, when $\tilde{\eta}_H$ is positive then Hall diffusion acts to reduce the net radial diffusion, resulting in magnetic walls and subshocks that disrupt the flow. The magnetic field carried inwards increases, and the magnetic pressure and tension terms remain important throughout the collapse. Any twist in the field lines causes an increase in the magnetic pressure gradient, so that the net amount of radial diffusion drops off as the magnetic braking slows the rotation.

There is a similar duality to the azimuthal field drift. Again looking at the region between the two shocks, when $\tilde{\eta}_H$ is negative Hall drift occurs in the azimuthal direction, twisting up the field lines in the pseudodisc and creating a leading torque on the neutral rotation. The reduced value of B_z causes the azimuthal field component to reach its capped value $B_{\phi,s} = -\delta B_z$ sooner, and the magnetic braking, which depends upon $B_z B_{\phi,s}$, is also reduced. Because of this less angular momentum is removed from the pseudodisc, causing the centrifugal force to become dynamically important earlier and a larger rotationally-supported disc to form.

In the other orientation when $\tilde{\eta}_H$ is positive, Hall and

Table 2. The surface density and vertical field component in the Keplerian disc at $r = 1$ au, the protostellar mass and the size and mass of the Keplerian disc at $t = 10^4$ years for the solutions depicted in Fig. 10.

| $\tilde{\eta}_H$ | Σ (g cm $^{-2}$) | B_z (G) | M_c (M_\odot) | M_{disc} (M_\odot) | R_c (au) |
|------------------|--------------------------|-----------|-----------------------|--------------------------|------------|
| -0.2 | 1920 | 0.289 | 7.21×10^{-2} | 9.99×10^{-3} | 15.10 |
| 0 | 1250 | 0.299 | 7.62×10^{-2} | 3.75×10^{-3} | 5.31 |
| 0.2 | 620 | 0.304 | 7.54×10^{-2} | 1.24×10^{-3} | 2.43 |

ambipolar diffusion act together to untwist the field lines in the pseudodisc. In these similarity solutions B_z is larger, and so while it takes longer for $B_{\phi,s}$ to achieve its capped value there is more magnetic braking and the angular momentum is further reduced. A smaller Keplerian disc forms due to the reduced centrifugal force, and both shocks have subshocks where the magnetic forces alter the radial velocity of the fluid. Downstream of the magnetic diffusion shock the radial magnetic pressure gradient slows the fluid in the radial and azimuthal directions, while downstream of the centrifugal shock the gas is accelerated inward as the increase in B_z causes a burst of magnetic braking that disrupts the disc and causes the formation of a subshock.

While the angular momentum behaviour between the shocks is changed by the inclusion of Hall diffusion, the cap on $B_{\phi,s}$ acts to ensure that the angular momentum in the inner disc is that expected for a Keplerian disc. The cap, while physically motivated, replaces unspecified disc physics such as reconnection, a disc wind, or turbulence, which would act to prevent the azimuthal field component from greatly exceeding the vertical component; and the magnitude at which it ought to act to limit $B_{\phi,s}$ is uncertain. It is also unclear if such limiting of the azimuthal field component happens in real collapsing cores, as numerical simulations do demonstrate tightly-wound magnetic fields (e.g. Machida et al. 2008b). The azimuthal field cap limits the similarity solution set explored to those in which discs form, however despite this Hall diffusion has been shown to restrict disc formation in collapse without counter-rotation if the Hall diffusion is too strong in comparison to ambipolar diffusion and $\tilde{\eta}_H$ has the “wrong” sign. If the core was initially rotating in the opposite direction, the opposite sign of $\tilde{\eta}_H$ would be problematic to disc formation.

All of the solutions in Fig. 10 and Braiding (2011) form protostars of around 0.7 solar masses with protostellar discs of radius $R_c \sim 10$ –150 au and mass $M_d \sim 10^{-2}$ – $10^{-1} M_\odot$ in $t = 10^5$ years; these are the same order of magnitude expected from observations of Class I YSOs (e.g. Jørgensen et al. 2007). The surface density of the disc is quite sensitive to the Hall diffusion parameter, and scales as $\Sigma \propto r^{-3/2}$ and $\Sigma \propto t^{1/2}$ in the inner Keplerian disc, with values $\Sigma(r = 1 \text{ au}, t = 10^4 \text{ years}) \sim 10^3 \text{ g cm}^{-2}$ (see Table 2). These values of the surface density are consistent with what is thought to have occurred in the solar nebula (e.g. the minimum mass solar nebula has $\Sigma = 1700 \text{ g cm}^{-2}$ at $r = 1 \text{ au}$; Weidenschilling 1977).

It has recently been argued that there exists a hand- edness to observations of transverse gradients in the Faraday rotation measure across the base of jets associated with active galactic nuclei (AGN; Contopoulos et al. 2009). The majority of sources in which it was possible to determine the transverse gradients were found to have clockwise gradients, implying that the outflow has a helical magnetic field

with a preferred magnetic polarity. One explanation of this behaviour is that the Hall effect is important in the inner accretion disc, acting to form a jet when the field has a positive magnetic polarity, and to suppress jet formation when the polarity is negative (Königl 2010). This explanation fits the limited available data well, although it must be confirmed by future observations at higher resolutions and sensitivities.

Similarly, it may be possible to show the importance of the sign of the Hall parameter observationally by measuring the polarisation of the magnetic field with respect to the axis of rotation in Zeeman observations of newly-forming stars and their discs. Should larger discs and lower accretion rates be correlated with a particular field orientation then the Hall effect will have been shown to affect the collapse process. ALMA (among other next-generation instruments) shall be capable of imaging nearby dense prestellar cores and their envelopes in both dust and molecular line emission, and could also be used to observe polarised dust emission and map the magnetic field in cores. Such observations could be sensitive enough to observe if there is any difference in the field alignment between protostellar discs and their envelopes, and whether there is any correlation between disc size and the direction of rotation in the disc.

None of the solutions calculated the effects of very weak magnetic diffusion or strong magnetic braking on the core. In numerical simulations with such conditions the magnetic braking removes all of the angular momentum from the fluid, preventing the formation of a rotationally-supported disc – this behaviour has been dubbed the “magnetic braking catastrophe” (see e.g. Allen et al. 2003b; Mellon & Li 2008, 2009; Hennebelle & Ciardi 2009; Li et al. 2011). Disc formation was assured in this work by the cap placed upon $B_{\phi,s}$, which limits the twisting of the field lines, however KK02 were able to demonstrate the magnetic braking catastrophe by adopting a large δ . Hall diffusion is capable of inducing spin in an initially-nonrotating fluid (Wardle & Ng 1999), and could resolve the magnetic braking catastrophe in solutions with strong braking by spinning up the core in the opposite direction once magnetic braking has removed the initial angular momentum. Hall-induced spin-up of an initially-nonrotating core was demonstrated by Krasnopolsky et al. (2011), although the formation of a Keplerian disc required a larger Hall parameter than that expected from the microphysics, possibly because the 10 au sink particle prevented the outwards growth of a disc from the geometric centre of the collapse.

Further work must be done to study the role of the Hall effect on the magnetic field diffusion in star formation, particularly using the semianalytic model constructed in this work. This could include adopting more realistic values and scalings of the ambipolar and Hall diffusion parameters, in order to resolve the magnetic braking catastrophe; including a disc wind in place of the cap on $B_{\phi,s}$; and exploring those

regions of parameter space in which Hall diffusion is the dominant form of field transport.

As explained in §2.1, the Hall and ambipolar diffusion coefficients in our calculations scale with the nondimensional variables in the same manner. However, the diffusion coefficients could scale as any function of x and the self-similar variables in order to mimic the behaviour expected from ionisation equilibrium calculations. For example, the Hall parameter could scale as

$$\frac{\eta'_H}{b} = \tilde{\eta}_H \sqrt{\frac{h}{\sigma}}, \quad (92)$$

which is expected if the only particles in the collapsing core are neutrals and ions, without grains. Such a formulation would cause Hall diffusion to become important earlier in the collapse, and the Keplerian disc would need to be described by a new set of asymptotic inner boundary conditions.

The inner Keplerian disc in our solutions satisfies the criterion $B_{r,s}/B_z > 1/\sqrt{3}$, which is the launching condition for a cold, centrifugally-driven wind, and the radial scaling of the magnetic field components is identical to that of the radially-self-similar wind solution of Blandford & Payne (1982). Such a disc wind (described in appendix C of KK02) would be the dominant mechanism for the vertical transfer of angular momentum from the disc to the envelope, and must be included in future self-similar collapse simulations in order to explore the influence a wind may have on the angular momentum transport and the magnetic braking catastrophe, and to improve the accuracy of the semianalytic models, as disc winds and jets occur in numerical simulations of collapsing cores (e.g. Tomisaka 2002; Mellon & Li 2009; Ciardi & Hennebelle 2010), some of which display the magnetic braking catastrophe.

Further explorations of parameter space are required to more fully understand the influence of the Hall effect on star and Keplerian disc formation. In particular we have yet to fully separate the influence of Hall diffusion from that of increased ambipolar diffusion in the core, to find similarity solutions in which Hall diffusion is the dominant form of flux transport, or solutions in which there is no ambipolar diffusion at all. As in Krasnopolsky et al. (2011), solutions with only Hall diffusion see the field diffusion depend upon the $\mathbf{J} \times \mathbf{B}$ terms, so the radial diffusion is controlled by the azimuthal field component (which may be capped), and the azimuthal diffusion depends upon the radial component. Additional work should also be done to confirm that larger discs form in Hall similarity solutions where the core is initially rapidly-rotating.

6 CONCLUSIONS

This paper described a semianalytic self-similar model of the gravitational collapse of rotating magnetic molecular cloud cores with both Hall and ambipolar diffusion, presenting similarity solutions that showed that the Hall effect has a profound influence on the dynamics of collapse. The solutions satisfied the vertically-averaged self-similar equations for MHD collapse under the assumptions of axisymmetry and isothermality, matching onto self-similar power law relations describing an isothermal core at the moment of point

mass formation on the outer boundary and a Keplerian disc on the inner boundary.

The inner solution describes a Keplerian disc in which accretion through the disc depends upon the magnetic diffusion; with an appropriate value of the nondimensional Hall diffusion parameter $\tilde{\eta}_H$ a stable rotationally-supported disc forms in which the surface density Σ scales as $r^{-3/2}$ and vertical field strength $B_z \propto r^{-5/4}$. These are the scalings expected from other simulations of protostellar discs to which the solutions calculated in this work compare favourably. No disc may form in solutions without counter-rotation when the Hall parameter is large (in comparison to the ambipolar diffusion parameter) and has the wrong sign (which indicates the orientation of the magnetic field with respect to the axis of rotation), as the diffusion in these solutions is too strong and causes disruptive torques that form subshocks in the similarity solutions. This behaviour occurs because the response of the fluid to Hall diffusion is not invariant under a global reversal of the magnetic field.

The size of the rotationally-supported disc in the full similarity solutions was shown to vary with the amount of Hall and ambipolar diffusion affecting the pseudodisc through their effect on the magnetic braking in the fluid. By creating an additional torque on the disc, Hall diffusion can either increase or decrease the angular momentum and rotational support in the infalling fluid, leading to an order of magnitude change in the Keplerian disc radius between the similarity solutions at the extremes of $-0.5 \leq \tilde{\eta}_H/\tilde{\eta}_A \leq 0.2$ (where the ambipolar diffusion parameter, $\tilde{\eta}_A = 1$). A small amount of Hall diffusion was shown have a large effect on the solution because the dynamic range of collapse is itself many orders of magnitude in space and time. Hall diffusion causes there to be a preferred handedness to the field alignment and the direction of rotation in forming a large Keplerian disc that could be observed using next-generation instruments such as ALMA.

The accretion rate onto the central point mass is similarly influenced by Hall diffusion. This is a smaller effect than that on the disc radius, as between $\tilde{\eta}_H = \pm 0.1\tilde{\eta}_A$ (again with $\tilde{\eta}_A = 1$) the accretion rate onto the protostar only changes by 6 per cent, or $0.2 \times 10^{-6} \text{ M}_\odot \text{ yr}^{-1}$. There exists a clear trend in which the protostellar accretion rate drops off with increasingly negative Hall parameter despite the constant accretion onto the core, as the reduced magnetic braking in these solutions causes a larger Keplerian disc to form, and accretion through this disc onto the protostar is slow.

The magnetic braking catastrophe could be resolved by the inclusion of Hall diffusion in numerical solutions, as with one sign of $\tilde{\eta}_H$ the Hall effect acts to reduce the total amount of braking affecting the core, preventing it from removing too much angular momentum from the collapse. However, with the other sign of $\tilde{\eta}_H$ the magnetic braking is increased so that more angular momentum is transported to the envelope. As magnetic braking due to Hall diffusion does not stop acting once no angular momentum remains (as ambipolar diffusion does) it could also then spin the collapsing fluid back up in the opposite direction to the initial rotation. This acceleration is only possible with Hall diffusion, and it has the potential to completely resolve the magnetic braking catastrophe.

Because of its tendency to move the magnetic field in

unusual directions Hall diffusion is usually overlooked in simulations of gravitational collapse and star formation. It has been shown that the Hall effect is important to the dynamics of the collapse, particularly the magnetic braking behaviour which determines the existence and size of the rotationally-supported protostellar disc. The handedness of the response of the collapse to the inclusion of the Hall effect has obvious dynamical and potentially observable consequences for the gravitational collapse of molecular cloud cores, which must be studied more closely if the dynamics of the star formation process and the variations observed across YSOs and their discs are to be properly understood.

ACKNOWLEDGMENTS

The authors wish to thank Ruben Krasnopolsky for his helpful comments on the numerical problems and counter-rotation, and the participants of the Dynamics of Discs and Planets Programme at the Isaac Newton Institute for Mathematical Sciences for the engaging and stimulating discussions. This work was supported in part by the Australian Research Council grant DP0881066.

REFERENCES

- Adams F. S., Shu F. H., 2007, *ApJ*, 671, 497
 Allen A., Li Z.-Y., Shu F. H., 2003, *ApJ*, 599, 363
 Allen A., Shu F. H., Li Z.-Y., 2003, *ApJ*, 599, 351
 Attard M., Houde M., Novak G., Li H., Vaillancourt J. E., Dowell C. D., Davidson J., Shinnaga H., 2009, *ApJ*, 702, 1584
 Ballesteros-Paredes J., Klessen R. S., Mac Low M.-M., Vázquez-Semadeni E., 2007, in Reipurth B., Jewitt D., Keil K., eds, *PPV*, Univ. Arizona Press
 Basu S., 1997, *ApJ*, 485, 240
 Basu S., Mouschovias T. Ch., 1994, *ApJ*, 432, 720
 Blandford R. D., Payne D. G., 1982, *MNRAS*, 199, 883
 Braiding C. R., 2011, PhD thesis, Macquarie University
 Chandrasekhar S., Fermi E., 1953, *ApJ*, 118, 116
 Ciardi A., Hennebelle P., 2010, *MNRAS*, 409, L39
 Ciolek G. E., Königl A., 1998, *ApJ*, 504, 257
 Ciolek G. E., Mouschovias T. Ch., 1998, *ApJ*, 504, 280
 Contopoulos I., Christodoulou D. M., Kazanas D., Gabuzda D. C., 2009, *ApJL*, 702, L148
 Contopoulos I., Ciolek G. E., Königl A., 1998, *ApJ*, 504, 247
 Cortes P., Crutcher R. M., 2006, *ApJ*, 639, 965
 Crutcher R. M., 1999, *ApJ*, 520, 706
 Crutcher R. M., Hakobian N., Troland T. H., 2009, *ApJ*, 692, 844
 Desch S. J., Mouschovias T. Ch., 2001, *ApJ*, 550, 314
 Elmegreen B. G., 1979, *ApJ*, 232, 729
 Federrath C., Banerjee R., Clark P. C., Klessen R. S., 2010, *ApJ*, 713, 269
 Fiedler R. A., Mouschovias T. Ch., 1992, *ApJ*, 391, 199
 Fiedler R. A., Mouschovias T. Ch., 1993, *ApJ*, 415, 680
 Galli D., Lizano S., Shu F. H., Allen A., 2006, *ApJ*, 647, 374
 Galli D., Shu F. H., 1993, *ApJ*, 417, 220
 Galli D., Shu F. H., 1993, *ApJ*, 417, 243
 Gaustad J. E., 1963, *ApJ*, 138, 1050
 Girart J. M., Rao R., Marrone D. P., 2006, *Science*, 313, 812
 Gonçalves J., Galli D., Girart J. M., 2008, *A&A*, 490, L39
 Goodman A. A., Benson P. J., Fuller G. A., Myers P. C., 1993, *ApJ*, 406, 528
 Hennebelle P., Ciardi A., 2009, *A&A*, 506, L29
 Jørgensen J. K. et al., 2007, *ApJ*, 659, 479
 Kamaya H., Nishi R., 2000, *ApJ*, 543, 257
 Kane B. D., Clemens D. P., 1997, *AJ*, 112, 1799
 Königl A., 1989, *ApJ*, 342, 208
 Königl A., 2010, *MNRAS*, 407, L79
 Königl A., Salmeron R., 2011, in Garcia P. J. V., ed, *Physical Processes in Circumstellar Disks around Young Stars*, Univ. Chicago Press, Chicago
 Krasnopolsky R., Königl A., 2002, *ApJ*, 580, 987
 Krasnopolsky R., Li Z.-Y., Shang H., 2011, *ApJ*, 733, 54
 Larson R. B., 1969, *MNRAS*, 145, 271
 Lazarian A., 2005, *AIP Conference Series*, 784, 42
 Lee C., Ho P. T. P., White S. M., 2005, *ApJ*, 619, 948
 Lee C. W., Myers P. C., Tafalla M., 2001, *ApJS*, 136, 703
 Li Z.-Y., 1998, *ApJ*, 497, 850
 Li Z.-Y., Krasnopolsky R., Shang H., 2011, *ApJ*, 730, 180
 Li Z.-Y., McKee C. F., 1996, *ApJ*, 464, 373
 Machida M. N., Inutsuka S., Matsumoto T., 2008, *ApJ*, 676, 1088
 Machida M. N., Matsumoto T., Inutsuka S., 2008, *ApJ*, 685, 690
 McKee C. F., Zweibel E. G., Goodman A. A., Heiles C., 1993, in Levy E. H., Lunine J. I., eds, *PPIII*, Univ. Arizona Press
 Mac Low M.-M., Klessen R. S., 2004, *Rev. Modern Phys.*, 76, 125
 Mellon R. R., Li Z.-Y., 2008, *ApJ*, 682, 1356
 Mellon R. R., Li Z.-Y., 2009, *ApJ*, 698, 922
 Mestel L., Spitzer L. Jr., 1956, *MNRAS*, 116, 503
 Mouschovias T. Ch., Spitzer L. Jr., 1976, *ApJ*, 210, 326
 Mouschovias T. Ch., Tassis K., 2009, *MNRAS*, 400, L15
 Nakano T., Nakamura T., 1978, *PASJ*, 30, 671
 Penston M. V., 1969, *MNRAS*, 144, 425
 Saigo K., Hanawa T., 1998, *ApJ*, 493, 342
 Salmeron R., 2009, in Short W., Cairns I., eds, *Australian Space Science Conference Series: 8th Conference Proceedings*, National Space Society of Australia Ltd
 Salmeron R., Königl A., Wardle M., 2011, *MNRAS*, 412, 1162
 Sano T., Stone J. M., 2002, *ApJ*, 570, 314
 Sano T., Stone J. M., 2002, *ApJ*, 577, 534
 Shu F. H., 1977, *ApJ*, 214, 488
 Shu F. H., Adams F. C., Lizano S., 1987, *ARA&A*, 25, 23
 Shu F. H., Galli D., Lizano S., Cai M., 2006, *ApJ*, 647, 382
 Tasker E. J., Tan J. C., 2009, *ApJ*, 700, 358
 Tomisaka K., 2002, *ApJ*, 575, 306
 Toomre A., 1964, *ApJ*, 139, 1217
 Vink J. S., Drew J. E., Harries T. J., Oudmaijer R. D., Unruh Y., 2005, *MNRAS*, 359, 1049
 Wardle M., 2004, *Ap&SS*, 292, 317
 Wardle M., 2004, in Burton M., Jayawardhana R., Bourke T. eds, *Proc. IAU Symp. 221: Star Formation at High Angular Resolution*, Cambridge University Press
 Wardle M., 2007, *Ap&SS*, 311, 81
 Wardle M., Königl A., 1993, *ApJ*, 410, 218

- Wardle M., Ng C., 1999, MNRAS, 303, 329
Weidenschilling S. J., 1977, Ap&SS, 51, 153
Whitworth A., Summers D., 1985, MNRAS, 214, 1

APPENDIX A: VERTICAL AVERAGING

In order to produce a set of disc equations that depend only upon r and t , we average Equations 7–12 vertically over the disc in order to reduce the dimensionality of the problem. As the equations for the conservation of mass, radial and angular momentum and the vertical hydrostatic balance remain unchanged from KK02, the reader is directed to their appendix A or §2.3 of Braiding (2011) for the details of this averaging, and present here only the derivations of the vertically-averaged induction equation and the azimuthal field component.

A1 z -component of the induction equation

The z -component of the induction equation, given in Equation 12, is expanded more completely as

$$\frac{\partial B_z}{\partial t} = -\frac{1}{r} \frac{\partial}{\partial r} \left[r \left(V_r B_z + \eta \left(\frac{\partial B_r}{\partial z} - \frac{\partial B_z}{\partial r} \right) + \frac{\eta_H}{B} \left(B_z \frac{\partial B_\phi}{\partial z} + \frac{B_r}{r} \frac{\partial}{\partial r} (r B_\phi) \right) - \frac{\eta_A}{B^2} \left((B_z^2 + B_r^2) \left(\frac{\partial B_z}{\partial r} - \frac{\partial B_r}{\partial z} \right) - B_r B_\phi \frac{\partial B_\phi}{\partial z} + \frac{B_z B_\phi}{r} \frac{\partial}{\partial r} (r B_\phi) \right) \right) \right]. \quad (\text{A1})$$

The magnetic flux enclosed within a radius r is given by

$$\Psi(r) = \Psi_c + 2\pi \int_0^r B_z(r') r' dr', \quad (\text{A2})$$

where Ψ_c is the flux within the central point mass. This equation is then rewritten in differential form as

$$B_z = \frac{1}{2\pi r} \frac{\partial \Psi}{\partial r}, \quad (\text{A3})$$

and its derivative with respect to time is

$$\frac{\partial B_z}{\partial t} = \frac{1}{2\pi r} \frac{\partial}{\partial r} \left(\frac{\partial \Psi}{\partial t} \right). \quad (\text{A4})$$

This is substituted into Equation A1 and the partial derivative with respect to r and the factor of r^{-1} are cancelled to obtain

$$\frac{1}{2\pi} \frac{\partial \Psi}{\partial t} = -r \left[V_r B_z + \eta \left(\frac{\partial B_r}{\partial z} - \frac{\partial B_z}{\partial r} \right) + \frac{\eta_H}{B} \left(B_z \frac{\partial B_\phi}{\partial z} + \frac{B_r}{r} \frac{\partial}{\partial r} (r B_\phi) \right) - \frac{\eta_A}{B^2} \left((B_z^2 + B_r^2) \left(\frac{\partial B_z}{\partial r} - \frac{\partial B_r}{\partial z} \right) - B_r B_\phi \frac{\partial B_\phi}{\partial z} + \frac{B_z B_\phi}{r} \frac{\partial}{\partial r} (r B_\phi) \right) \right]. \quad (\text{A5})$$

The η and $\eta_{H,A}$ terms depend on $B^{0,1,2}$ respectively, so the leading fractions of the diffusive terms may be ignored as the integration over z is performed.

The flux, magnetic force and Ohmic diffusion terms are integrated over the disc height to give:

$$\int_{-\infty}^{+\infty} \frac{1}{2\pi} \frac{\partial \Psi}{\partial t} dz = \left[\frac{1}{2\pi} \frac{\partial \Psi}{\partial t} z \right]_{-H}^{+H} = \frac{2H}{2\pi} \frac{\partial \Psi}{\partial t}; \quad (\text{A6})$$

$$\int_{-\infty}^{+\infty} V_r B_z dz = \left[V_r B_z z \right]_{-H}^{+H} = 2H V_r B_z; \quad (\text{A7})$$

and

$$\int_{-\infty}^{+\infty} \left(\frac{\partial B_r}{\partial z} - \frac{\partial B_z}{\partial r} \right) dz = \int_{-H}^{+H} \frac{\partial}{\partial z} \left(\frac{B_{r,s} z}{H} \right) - \frac{\partial B_z}{\partial r} dz = 2 \left(B_{r,s} - H \frac{\partial B_z}{\partial r} \right). \quad (\text{A8})$$

The Hall diffusion terms are rearranged into the form

$$B_z \frac{\partial B_\phi}{\partial z} + \frac{B_r}{r} \frac{\partial}{\partial r} (r B_\phi) = \frac{\partial}{\partial z} (B_z B_\phi) - B_\phi \frac{\partial B_z}{\partial z} + \frac{B_r}{r} \frac{\partial}{\partial r} (r B_\phi); \quad (\text{A9})$$

and the vertical scaling of the azimuthal field component is substituted into the first term and the solenoidal condition (Equation 11) is applied to the second:

$$B_z \frac{\partial B_\phi}{\partial z} + \frac{B_r}{r} \frac{\partial}{\partial r} (r B_\phi) = \frac{\partial}{\partial z} \left(\frac{B_z B_{\phi,s} z}{H} \right) + \frac{B_\phi}{r} \frac{\partial}{\partial r} (r B_r) + \frac{B_r}{r} \frac{\partial}{\partial r} (r B_\phi). \quad (\text{A10})$$

The integral of the Hall terms may then be written as

$$\int_{-\infty}^{+\infty} \left[B_z \frac{\partial B_\phi}{\partial z} + \frac{B_r}{r} \frac{\partial}{\partial r} (r B_\phi) \right] dz = \int_{-\infty}^{+\infty} \left[\frac{\partial}{\partial z} \left(\frac{B_z B_{\phi,s} z}{H} \right) + \frac{1}{r^2} \frac{\partial}{\partial r} (r^2 B_r B_\phi) \right] dz, \quad (\text{A11})$$

which, after the vertical scalings of B_r and B_ϕ are substituted into it, is evaluated to give:

$$\begin{aligned} \int_{-\infty}^{+\infty} \left[B_z \frac{\partial B_\phi}{\partial z} + \frac{B_r}{r} \frac{\partial}{\partial r} (r B_\phi) \right] dz &= \left[\frac{B_z B_{\phi,s} z}{H} + \frac{z^3}{3r^2} \frac{\partial}{\partial r} \left(\frac{r^2 B_{r,s} B_{\phi,s}}{H^2} \right) \right]_{-H}^{+H} \\ &= 2B_z B_{\phi,s} + \frac{2H^3}{3r^2} \frac{\partial}{\partial r} \left(\frac{r^2 B_{r,s} B_{\phi,s}}{H^2} \right). \end{aligned} \quad (\text{A12})$$

Finally, the ambipolar diffusion terms are expanded out and integrated. The first of these terms is straightforward, as B_z is regarded as constant with height unless specifically differentiated with respect to z and may be taken outside of the integral, which is solved to obtain

$$\int_{-\infty}^{+\infty} (B_r^2 + B_z^2) \frac{\partial B_z}{\partial r} dz = \frac{\partial B_z}{\partial r} \int_{-H}^{+H} \left(\frac{B_{r,s}^2 z^2}{H^2} + B_z^2 \right) dz = 2H \frac{\partial B_z}{\partial r} \left(\frac{B_{r,s}^2}{3} + B_z^2 \right). \quad (\text{A13})$$

The second of the ambipolar diffusion terms is rearranged into the form

$$(B_r^2 + B_z^2) \frac{\partial B_r}{\partial z} = B_r^2 \frac{\partial B_r}{\partial z} + B_z \frac{\partial}{\partial z} (B_r B_z) - B_r B_z \frac{\partial B_z}{\partial z} \quad (\text{A14})$$

to which the solenoidal condition (Equation 11) and the scalings for the other field components are applied. The integral of this term is then

$$\int_{-\infty}^{+\infty} (B_r^2 + B_z^2) \frac{\partial B_r}{\partial z} dz = \int_{-\infty}^{+\infty} \frac{B_{r,s}^2 z^2}{H^2} \frac{\partial}{\partial z} \left(\frac{B_{r,s} z}{H} \right) + B_z \frac{\partial}{\partial z} \left(\frac{B_{r,s} B_z z}{H} \right) + \frac{B_{r,s} B_z z^2}{Hr} \frac{\partial}{\partial r} \left(\frac{r B_{r,s}}{H} \right) dz; \quad (\text{A15})$$

this is evaluated over the height of the disc to give

$$\begin{aligned} \int_{-\infty}^{+\infty} (B_r^2 + B_z^2) \frac{\partial B_r}{\partial z} dz &= \left[\frac{B_{r,s}^3 z^3}{3H^3} + \frac{B_z^2 B_{r,s} z}{H} + \frac{B_{r,s} B_z z^3}{3rH} \frac{\partial}{\partial r} \left(\frac{r B_{r,s}}{H} \right) \right]_{-H}^{+H} \\ &= \frac{2}{3} B_{r,s}^3 + 2B_z^2 B_{r,s} + \frac{2}{3} H^2 B_{r,s}^2 B_z \left[\frac{d}{dr} [\ln(r B_{r,s})] - \frac{d}{dr} [\ln H] \right]. \end{aligned} \quad (\text{A16})$$

The third of the ambipolar diffusion terms is again straightforward; it is vertically-averaged by applying the vertical scalings to the radial and azimuthal components to the field and then performing the integral over z to find

$$\int_{-\infty}^{+\infty} B_r B_\phi \frac{\partial B_\phi}{\partial z} dz = \int_{-\infty}^{+\infty} \frac{B_{r,s} B_{\phi,s} z^2}{H^2} \frac{\partial}{\partial z} \left(\frac{B_{\phi,s} z}{H} \right) dz = \frac{2}{3} B_{r,s} B_{\phi,s}^2. \quad (\text{A17})$$

Finally, the last of the ambipolar diffusion terms in Equation A5 is averaged by substituting in the vertical scalings of the field components and then performing the integral:

$$\begin{aligned} \int_{-\infty}^{+\infty} \frac{B_\phi B_z}{r} \frac{\partial}{\partial r} (r B_\phi) dz &= \int_{-\infty}^{+\infty} \frac{B_{\phi,s} B_z z}{rH} \frac{\partial}{\partial r} \left(\frac{r B_{\phi,s} z}{H} \right) dz \\ &= \frac{2}{3} B_z B_{\phi,s}^2 H \left[\frac{d}{dr} [\ln(r B_{\phi,s})] - \frac{d}{dr} [\ln H] \right]. \end{aligned} \quad (\text{A18})$$

Collecting all of these integrated terms into the same order as in Equation A5 then gives the full vertically-averaged induction equation:

$$\begin{aligned} \frac{H}{2\pi} \frac{\partial \Psi}{\partial t} &= -r \left[H V_r B_z + \eta \left(B_{r,s} - H \frac{\partial B_z}{\partial r} \right) + \frac{\eta_H}{B} \left(B_z B_{\phi,s} + \frac{H^3}{3r^2} \frac{\partial}{\partial r} \left(\frac{r^2 B_{r,s} B_{\phi,s}}{H^2} \right) \right) \right. \\ &\quad - \frac{\eta_A}{B^2} \left[\left(B_{r,s} - H \frac{\partial B_z}{\partial r} \right) \left(B_z^2 + \frac{1}{3} B_{r,s}^2 \right) - \frac{1}{3} B_{\phi,s}^2 B_{r,s} \right. \\ &\quad \left. \left. + \frac{1}{3} H B_z B_{\phi,s}^2 \left(\frac{d}{dr} [\ln(r B_{\phi,s})] - \frac{d}{dr} [\ln H] \right) - \frac{1}{3} H B_z B_{r,s}^2 \left(\frac{d}{dr} [\ln(r B_{r,s})] - \frac{d}{dr} [\ln H] \right) \right] \right]. \end{aligned} \quad (\text{A19})$$

It is clear from this equation that the azimuthal field is pivotal in causing Hall drift in the radial direction; $B_{\phi,s}$ should not be neglected, even in axisymmetric models.

A2 Azimuthal field component

The vertical angular momentum transport above and within the pseudodisc is achieved by magnetic braking, especially during the dynamic collapse phase inwards of the magnetic diffusion shock. It is assumed that magnetic braking remains the dominant angular momentum transport mechanism during the subsequent evolution of the core, although it is likely that a centrifugally-driven disc wind may dominate in the innermost Keplerian disc. The approach to modelling the magnetic braking adopted here is adapted from that of Basu & Mouschovias (1994) for the pre-point mass formation collapse phase. This formulation is not well-defined in the innermost rotationally-supported regions of the disc, where the calculated magnetic braking becomes

stronger than is expected and the angular momentum transport is expected to be dominated by a disc wind (this is discussed in more detail in §5). A cap is then placed upon the azimuthal magnetic field component in order to ensure that it does not greatly exceed the vertical component; because of this the magnetic braking prescription is not expected to introduce significant errors into the inner regions of the calculations.

External to the pseudodisc the magnetic field is considered to be frozen into the low-density, constant-pressure external medium, which has density ρ_{ext} and angular velocity Ω_b . Within the external medium the magnetic field assumes the value $\mathbf{B} = B_{\text{ref}}\hat{z}$, and the exterior flux tubes corotate with the core. Because the transition region has a low moment of inertia relative to the core, and the crossing time for Alfvén waves is always much smaller than the evolutionary time of the core, the transition region can relax to a steady state during all stages of contraction (Basu & Mouschovias 1994).

The induction equation under IMHD implies

$$(B_p \cdot \nabla)\Omega = 0 \quad (\text{A20})$$

where B_p is the poloidal field, so that the angular velocity Ω is constant on a magnetic surface. The force equation is similarly

$$(B_p \cdot \nabla)rB_\phi = 0, \quad (\text{A21})$$

which further implies that rB_ϕ does not change along the field lines. The neutral particles carry the torque and angular momentum is carried upwards by torsional Alfvén waves generated by the rotation of the disc.

Over a period of time dt an amount of material equal to $2\pi\rho r_{\text{ref}}dr_{\text{ref}}$ moves from the undisturbed position $r_{\text{ref}}dr_{\text{ref}}$ in the external medium along a flux tube with angular velocity Ω to a radius rdr at the disc surface. The angular momentum of the gas goes as

$$dJ = -[2\pi\rho_{\text{ext}}r_{\text{ref}}dr_{\text{ref}}](V_{\text{A,ext}}dt)r_{\text{ref}}^2(\Omega - \Omega_b), \quad (\text{A22})$$

where $V_{\text{A,ext}}$, the external Alfvén speed, is given by

$$V_{\text{A,ext}} = \frac{B_{\text{ref}}}{\sqrt{4\pi\rho_{\text{ext}}}}. \quad (\text{A23})$$

For purely azimuthal motions in the external medium, the total angular momentum in each flux tube is conserved. This angular momentum must be removed from the disc at a rate equal to

$$\frac{dJ}{dt} = -2\pi r_{\text{ref}}^2 V_{\text{A,ext}} \rho_{\text{ext}} (\Omega - \Omega_b) r_{\text{ref}} dr_{\text{ref}}, \quad (\text{A24})$$

which gives a torque on the disc

$$N = -\frac{2\pi r_{\text{ref}}^2 (V_{\text{A,ext}} \rho_{\text{ext}}) (\Omega - \Omega_b) r_{\text{ref}} dr_{\text{ref}}}{\pi r dr}. \quad (\text{A25})$$

The amount of flux remains constant along flux tubes, so that the flux through the disc inside of a radius r is equal to the amount of flux through the cylindrical external cloud inside of the radius r_{ref} :

$$\Psi = \int_0^r 2\pi r' B_{z,eq}(r') dr' = \pi r_{\text{ref}}^2 B_{\text{ref}}, \quad (\text{A26})$$

where $B_{z,eq}$ is the value of B_z at the midplane of the disc. Thus

$$d\Psi = 2\pi r B_{z,eq} dr = 2\pi r_{\text{ref}} B_{\text{ref}} dr_{\text{ref}} \quad (\text{A27})$$

and

$$\frac{r_{\text{ref}} dr_{\text{ref}}}{r dr} = \frac{B_{z,eq}}{B_{\text{ref}}}, \quad (\text{A28})$$

so that the torque in Equation A25 becomes

$$N = -\frac{2\pi r_{\text{ref}}^2 (\Omega - \Omega_b) B_{z,eq}}{B_{\text{ref}}} \left(\frac{B_{\text{ref}} \rho_{\text{ext}}}{\sqrt{4\pi\rho_{\text{ext}}}} \right) = -\frac{(\Omega - \Omega_b) B_{z,eq} (\Psi/2\pi)}{\pi V_{\text{A,ext}}}. \quad (\text{A29})$$

The torque per unit area on the disc is given by

$$N = \frac{r B_{z,eq} B_{\phi,s}}{2\pi}, \quad (\text{A30})$$

combining Equations A29 and A30 gives the steady state azimuthal magnetic field component at the surface of the disc:

$$B_{\phi,s} = -\frac{\Psi}{\pi r^2} \frac{(r\Omega - r\Omega_b)}{V_{\text{A,ext}}} \quad (\text{A31})$$

(equation 26 of Basu & Mouschovias, 1994; equation 3 of KK02). It is clear that the properties of the external medium determine the conditions at the disc surface. This steady state approximation requires that the ratio of the Alfvén travel time in the external medium to the initial radius of the cloud be less than the evolutionary timescale, which scales with r as $\sim r/|V_r|$. For the rotationally-supported discs presented here $|V_r| \lesssim c_s$ (and $|V_r| \rightarrow 0$ as $r \rightarrow 0$), which is much smaller than

the Alfvén speed for the adopted gas temperature of 10K ($V_{A,\text{ext}} \approx 5c_s$); this implies that the assumption of rapid braking of the core should not introduce large errors into the solutions.

The angular velocity Ω is given by the equation

$$\Omega = \frac{1}{r}(V_\phi + V_{B\phi}), \quad (\text{A32})$$

where, using $\eta_P = \eta_A + \eta$,

$$V_{B\phi} = -\frac{1}{B} \left[\eta_H (\nabla \times \mathbf{B})_\perp - \eta_P (\nabla \times \mathbf{B})_\perp \times \hat{\mathbf{B}} \right]_\phi. \quad (\text{A33})$$

This equation is then expanded out to become

$$\begin{aligned} V_{B\phi} = & -\frac{1}{B^2} \left[\frac{\eta_H}{B} \left((B_z^2 + B_r^2) \left(\frac{\partial B_z}{\partial r} - \frac{\partial B_r}{\partial z} \right) + B_\phi B_z \frac{1}{r} \frac{\partial}{\partial r} (r B_\phi) - B_\phi B_r \frac{\partial B_\phi}{\partial z} \right) \right. \\ & \left. - \frac{\eta_P}{B^2} (B_r^2 + B_\phi^2 + B_z^2) \left(\frac{B_r}{r} \frac{\partial}{\partial r} (r B_\phi) + B_z \frac{\partial B_\phi}{\partial z} \right) \right], \end{aligned} \quad (\text{A34})$$

Most of the terms in this equation have direct analogies in Equation A5, and the individual steps of the vertical integration are not reproduced here. The vertical averaging gives

$$\begin{aligned} H V_{B\phi} \left(\frac{1}{3} B_{r,s}^2 + \frac{1}{3} B_{\phi,s}^2 + B_z^2 \right) = & -\frac{\eta_H}{B} \left[\left(\frac{B_{r,s}^2}{3} + B_z^2 \right) \left(B_{r,s} - H \frac{\partial B_z}{\partial r} \right) + \frac{1}{3} H B_z B_{r,s}^2 \left(\frac{d}{dr} [\ln(r B_{r,s})] - \frac{d}{dr} [\ln H] \right) \right. \\ & \left. + \frac{1}{3} B_{r,s} B_{\phi,s}^2 - \frac{1}{3} H B_z B_{\phi,s}^2 \left(\frac{d}{dr} [\ln(r B_{\phi,s})] - \frac{d}{dr} [\ln H] \right) \right] \\ & + \frac{\eta_P}{B^2} \left[B_z B_{\phi,s} \left(\frac{1}{3} B_{r,s}^2 + \frac{1}{3} B_{\phi,s}^2 + B_z^2 \right) \right. \\ & \left. + H B_{r,s} B_{\phi,s} \left(\frac{B_{r,s}^2}{5} + \frac{B_{\phi,s}^2}{5} + \frac{B_z^2}{3} \right) \left(\frac{d}{dr} [\ln(r B_{\phi,s})] + \frac{d}{dr} [\ln(r B_{r,s})] - 2 \frac{d}{dr} [\ln H] \right) \right]. \end{aligned} \quad (\text{A35})$$

This equation is simplified as in §2 by omitting any terms of order $\mathcal{O}(H/r)$ save for the $[B_{r,s} - H(\partial B_z/\partial r)]$ term; and the final form of $V_{B\phi}$ is then:

$$V_{B\phi} = -\frac{1}{H} \left[\frac{\eta_H}{B} \left(B_{r,s} - H \frac{\partial B_z}{\partial r} \right) - \frac{\eta_P}{B^2} B_z B_{\phi,s} \right]. \quad (\text{A36})$$

This is equivalent to the ion-neutral drift velocity adopted by KK02 (their equation 9), with the inclusion of terms describing the effect of Hall diffusion.

The Ω_b term is dropped from Equation A31, as the molecular cloud rotation rate is slow compared with that of the collapsing material. Rotation is dynamically important in the inner regions of the solutions presented in this thesis, while it is not important in most molecular clouds, so it is reasonable to declare that $\Omega \gg \Omega_b$ and dismiss Ω_b as small. The external Alfvén speed, $V_{A,\text{ext}}$, is treated as a constant with respect to the isothermal sound speed in these calculations, parameterised by the constant α (defined in Equation 19). This scaling of $V_{A,\text{ext}}$ is reasonable as the observations by Crutcher (1999) indicated that $V_A \approx 1 \text{ km s}^{-1}$ over at least four orders of magnitude in density ($\sim 10^3$ – 10^7 cm^{-3}) in their observed molecular clouds.

Equations A36 and 19 are substituted into 18 to find that

$$B_{\phi,s} = -\frac{\Psi\alpha}{\pi r^2 c_s} \left[\frac{J}{r} - \frac{\eta_H}{B} \left(B_{r,s} - H \frac{\partial B_z}{\partial r} \right) \right] \left[1 + \frac{\Psi\alpha}{\pi r^2 c_s} \frac{\eta_P}{B^2} \frac{B_z}{H} \right]^{-1}. \quad (\text{A37})$$

Note that B has an implied $B_{\phi,s}$ dependence; this is typically solved for numerically when calculating the azimuthal field.

For the inner solutions, Ω increases with decreasing r (proportional to $r^{-3/2}$); this would make $B_{\phi,s}$ the dominant field component at the surface near to the central point mass. Such behaviour is not expected in a real disc, where internal kinks of the field and magnetohydrodynamical instabilities (for example, the magnetorotational instability) should reduce the value of B_ϕ at the surface. An artificial limit on $B_{\phi,s}$ is imposed:

$$|B_{\phi,s}| \leq \delta B_z, \quad (\text{A38})$$

where δ is a parameter of the model usually chosen to be $\delta = 1$ in order to ensure that the azimuthal field component does not exceed the vertical component. KK02 point out that this value quite conveniently corresponds to that expected for a rotationally-supported disc where the vertical angular momentum transport is dominated by a centrifugally-driven wind. Applying this cap to Equation A37 then gives the final equation for $B_{\phi,s}$:

$$B_{\phi,s} = -\min \left[\frac{\Psi\alpha}{\pi r^2 c_s} \left[\frac{J}{r} - \frac{\eta_H}{B} \left(B_{r,s} - H \frac{\partial B_z}{\partial r} \right) \right] \left[1 + \frac{\Psi\alpha}{\pi r^2 c_s} \frac{\eta_P}{B^2} \frac{B_z}{H} \right]^{-1}; \delta B_z \right]. \quad (\text{A39})$$

This paper has been typeset from a $\text{\TeX}/\text{\LaTeX}$ file prepared by the author.